Science Signaling

18 March 2014

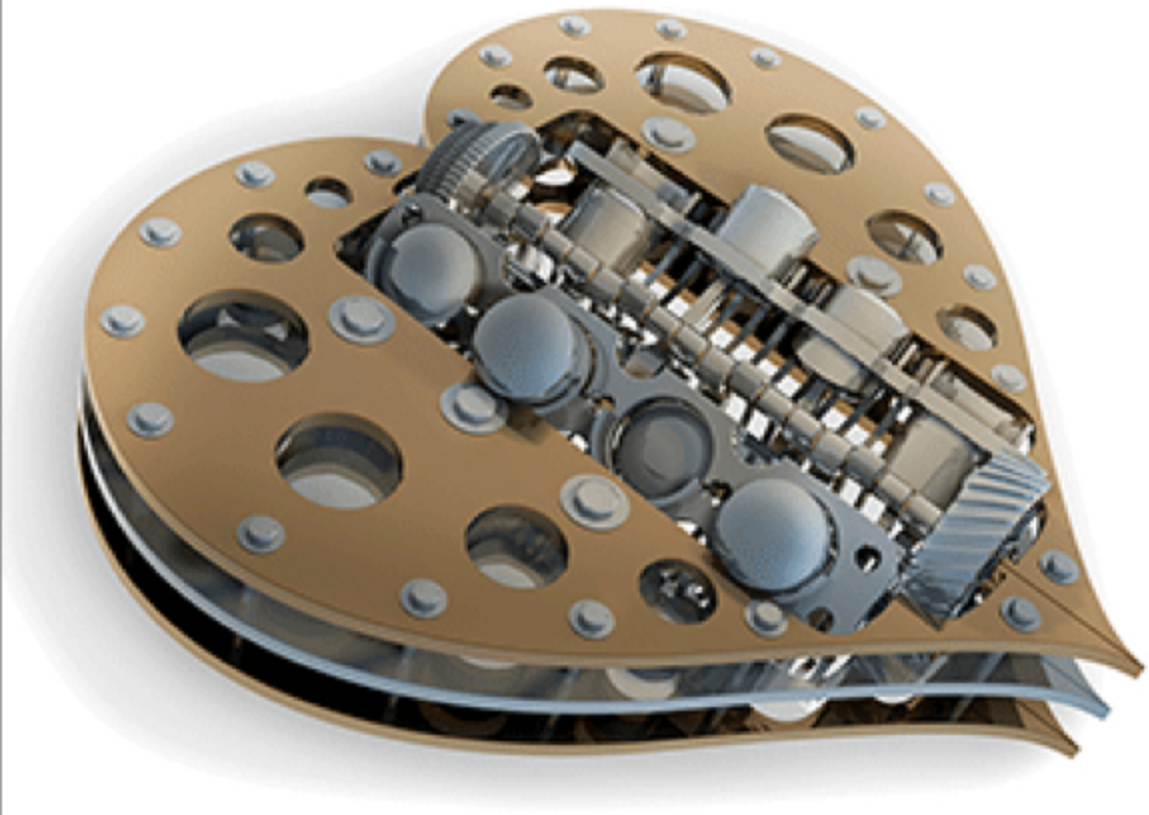

AAAS

Science Signaling
AAAS

# ` Mechanochemotransduction During Cardiomyocyte Contraction Is Mediated by Localized Nitric Oxide Signaling

Zhong Jian, Huilan Han, Tieqiao Zhang, Jose Puglisi, Leighton T. Izu, John A. Shaw, Ekama Onofiok, Jeffery R. Erickson, Yi-Je Chen, Balazs Horvath, Rafael Shimkunas, Wenwu Xiao, Yuanpei Li, Tingrui Pan, James Chan, Tamas Banyasz, Jil C. Tardiff, Nipavan Chiamvimonvat, Donald M. Bers, Kit S. Lam and Ye Chen-Izu (18 March 2014)
*Science Signaling* **7** (317), ra27. [DOI: 10.1126/scisignal.2005046]



*Science Signaling* (ISSN 1937-9145) is published weekly, except the last week in December, by the American Association for the Advancement of Science, 1200 New York Avenue, NW, Washington, DC 20005. 

CELL BIOLOGY

# Mechanochemotransduction During Cardiomyocyte Contraction Is Mediated by Localized Nitric Oxide Signaling

Zhong Jian,[1]* Huilan Han,[1]* Tieqiao Zhang,[2]* Jose Puglisi,[1] Leighton T. Izu,[1] John A. Shaw,[3] Ekama Onofiok,[4] Jeffery R. Erickson,[1] Yi-Je Chen,[1] Balazs Horvath,[1,5] Rafael Shimkunas,[1,6,7] Wenwu Xiao,[4] Yuanpei Li,[4] Tingrui Pan,[6] James Chan,[2] Tamas Banyasz,[1,5] Jil C. Tardiff,[8] Nipavan Chiamvimonvat,[7] Donald M. Bers,[1] Kit S. Lam,[4] Ye Chen-Izu[1,6,7]†

**Cardiomyocytes contract against a mechanical load during each heartbeat, and excessive mechanical stress leads to heart diseases. Using a cell-in-gel system that imposes an afterload during cardiomyocyte contraction, we found that nitric oxide synthase (NOS) was involved in transducing mechanical load to alter $Ca^{2+}$ dynamics. In mouse ventricular myocytes, afterload increased the systolic $Ca^{2+}$ transient, which enhanced contractility to counter mechanical load, but also caused spontaneous $Ca^{2+}$ sparks during diastole that could be arrhythmogenic. The increases in the $Ca^{2+}$ transient and sparks were attributable to increased ryanodine receptor (RyR) sensitivity because the amount of $Ca2^{+}$ in the sarcoplasmic reticulum load was unchanged. Either pharmacological inhibition or genetic deletion of nNOS (or NOS1), but not of eNOS (or NOS3), prevented afterload-induced $Ca2^{+}$ sparks. This differential effect may arise from localized NO signaling, arising from the proximity of nNOS to RyR, as determined by super-resolution imaging. $Ca^{2+}$-calmodulin–dependent protein kinase II (CaMKII) and nicotinamide adenine dinucleotide phosphate oxidase 2 (NOX2) also contributed to afterload-induced $Ca^{2+}$ sparks. Cardiomyocytes from a mouse model of familial hypertrophic cardiomyopathy exhibited enhanced mechanotransduction and frequent arrhythmogenic $Ca^{2+}$ sparks. Inhibiting nNOS and CaMKII, but not NOX2, in cardiomyocytes from this model eliminated the $Ca2^{+}$ sparks, suggesting mechanotransduction activated nNOS and CaMKII independently from NOX2. Thus, our data identify nNOS, CaMKII, and NOX2 as key mediators in mechanochemotransduction during cardiac contraction, which provides new therapeutic targets for treating mechanical stress–induced $Ca^{2+}$ dysregulation, arrhythmias, and cardiomyopathy.**

## INTRODUCTION

The heart must pump blood against mechanical loads that constantly change with physical activity, posture, emotion, and pathophysiological states. The Anrep effect (*1*–*4*) describes an enhancement of cardiac contractility resulting from increased afterload, which is complementary to the Frank-Starling mechanism that describes enhanced contractility from increased preload (*5*). Petroff *et al.* (*6*) have found that stretching cardiomyocytes to increase preload can induce spontaneous $Ca^{2+}$ sparks by activating the nitric oxide synthase 3 (or eNOS). Prosser *et al.* (*7*, *8*) have shown that stretching cardiomyocytes activates nicotinamide adenine dinucleotide phosphate oxidase 2 (NOX2) to cause $Ca^{2+}$ sparks. Preload-induced changes in $Ca^{2+}$ handling contribute to the Frank-Starling mechanism. However, it has been incompletely understood whether afterload might also cause changes in $Ca^{2+}$ handling and whether analogous mechanochemotransduction mechanisms could be activated in cardiomyocytes contracting against a mechanical load. Such knowledge is critical for understanding why excessive afterload under pathological conditions such as hypertension, infarction, and asynchronous contraction can lead to cardiac remodeling, hypertrophy, arrhythmias, and heart failure (*9*–*11*). Here, we identified nitric oxide synthase 1 (or nNOS), $Ca^{2+}$-calmodulin–dependent protein kinase II (CaMKII), and NOX2 as key mediators of mechanochemotransduction pathways that transduce mechanical afterload to $Ca^{2+}$ handling. These findings provide new mechanistic understanding of the Anrep effect and help to identify possible molecular targets for treating heart diseases that are induced by mechanical stress.

## RESULTS

### The cell-in-gel system to impose mechanical load during single cardiomyocyte contraction

Previously, investigations of mechanochemotransduction mechanisms have been limited by difficulties in controlling the mechanical load on cardiomyocyte contraction at the single-cell level. We developed a "cell-in-gel" system by embedding freshly isolated cardiomyocytes in a three-dimensional (3D) elastic matrix made of polyvinyl alcohol (PVA) hydrogel and boronic acid cross-linker; the boronate group also cross-linked the cell surface glycans, thereby tethering the cell surface to the gel (Fig. 1A and fig. S1) (*12*). This system has several advantages. When the in-gel cardiomyocyte contracts against the gel matrix, the elastic matrix resists the shortening and broadening of the cell during contraction, thereby exerting multiaxial

[1]Department of Pharmacology, University of California, Davis, Davis, CA 95616, USA. [2]Center for Biophotonics Science and Technology, University of California, Davis, Davis, CA 95616, USA. [3]Department of Aerospace Engineering, University of Michigan, Ann Arbor, MI 48109, USA. [4]Department of Biochemistry and Molecular Medicine, University of California, Davis, Davis, CA 95616, USA. [5]Department of Physiology, University of Debrecen, Medical and Health Science Centre, 4012 Debrecen, Hungary. [6]Department of Biomedical Engineering, University of California, Davis, Davis, CA 95616, USA. [7]Department of Internal Medicine (Cardiology), University of California, Davis, Davis, CA 95616, USA. [8]Department of Medicine, University of Arizona, Tucson, AZ 85721, USA.
*These authors contributed equally to this work.
†Corresponding author. E-mail: ychenizu@ucdavis.edu

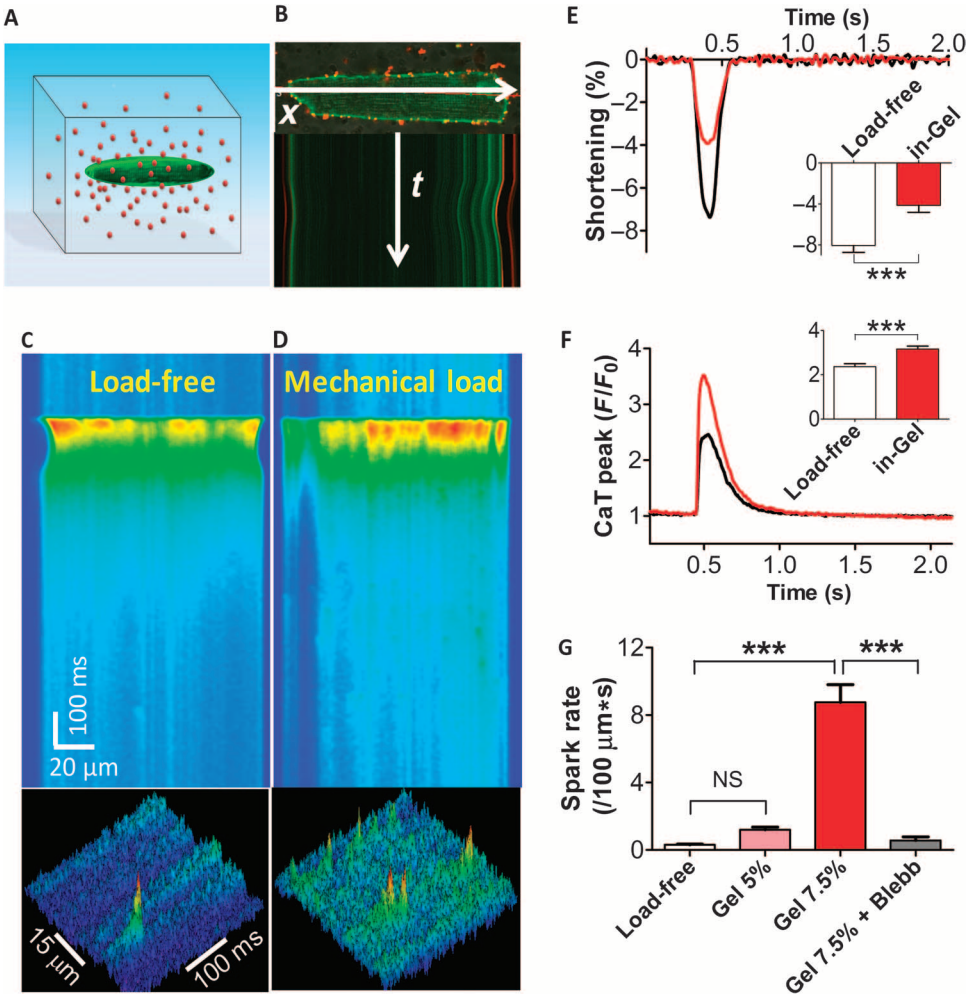


Fig. 1. The effects of mechanical stress on $Ca^{2+}$ handling during systole and diastole. (A) Schematic of a cardiomyocyte embedded in 3D hydrogel matrix containing red fluorescence beads. (B) Confocal imaging of a cardiomyocyte and beads demonstrating cell contraction and gel deformation as seen in the movement of the cell's edge and the red fluorescent beads embedded in gel. (C) Cardiomyocytes contracting in normal Tyrode solution were designated the load-free control. Confocal linescan image shows the $Ca^{2+}$ transient in bright fluorescence and the cell contraction in edge movement (upper panel); diastolic $Ca^{2+}$ sparks are few (lower panel). (D) Cardiomyocytes contracting in-gel under mechanical load. The $Ca^{2+}$ transient is high, and the cell contraction is small (upper panel); diastolic $Ca^{2+}$ sparks are increased (lower panel). (E) Fractional shortening of cardiomyocyte contraction in-gel ($n$ = 17 cells) compared with load-free control ($n$ = 17). (F) Systolic $Ca^{2+}$ transient (CaT) peak in cell-in-gel ($n$ = 17) compared with load-free control ($n$ = 17). (G) Diastolic $Ca^{2+}$ spark frequency in cardiomyocytes that were load-free ($n$ = 18) in soft gel made of 5% cross-linker (Gel 5%, $n$ = 9), in gel with 7.5% cross-linker (Gel 7.5%, $n$ = 18), and treated with blebbistatin (Blebb) ($n$ = 5). One-way analysis of variance (ANOVA) with Bonferroni posttest was used for pairwise comparison; ***$P$ < 0.001.

mechanical stress on the cell (Fig. 1B). Furthermore, the stiffness of the gel is tunable by the mixing ratio of the cross-linker and the PVA (*13*). In addition, the gel matrix is porous to allow rapid bath solution exchange for studying drug effects and is optically transparent for real-time imaging of cell contraction and fluorescence imaging of $Ca^{2+}$ signals. The gel components are nontoxic and do not affect the cell function (fig. S2). This cell-in-gel system mimics the in vivo mechanical environment in two aspects: the imposition of multiaxial 3D mechanical stress during contraction, and the tethering of the cell surface to the gel to impose both normal and shear stresses to the cell surface (*14*).

## Afterload-induced changes in $Ca^{2+}$ handling during systole and diastole

We studied the effects of mechanical stress during cardiomyocyte contraction under mechanical afterload using the cell-in-gel system. The cardiomyocyte was paced at 0.5 Hz to reach steady-state contraction (movie S1) while being continuously perfused with Tyrode solution. Compared to load-free contractions (Fig. 1C), the cardiomyocyte contracting in-gel (Fig. 1D) displayed less fractional shortening (Fig. 1E); it also showed augmented $Ca^{2+}$ transient in systole (Fig. 1F), as well as spontaneous $Ca^{2+}$ sparks during diastole (Fig. 1G). The $Ca^{2+}$ spark rate (sparks per unit area) was low under load-free condition, slightly increased in soft gel (Gel 5%), and significantly increased in stiffer gel (Gel 7.5%). Decoupling contraction from $Ca^{2+}$ signaling using the myosin II inhibitor blebbistatin reduced the $Ca^{2+}$ spark rate to that of the load-free condition (Fig. 1G). These data demonstrate a positive correlation between the mechanical load and the spontaneous $Ca^{2+}$ spark rate. We also examined the systolic $Ca^{2+}$ transient and cardiomyocyte contraction under the above conditions of varying loads. Compared to load-free contraction, cardiomyocyte contraction in soft gel (Gel 5%) under moderate mechanical load did not significantly alter the $Ca^{2+}$ transient; however, cardiomyocyte contraction in stiffer gel (Gel 7.5%) under higher mechanical load significantly increased the $Ca^{2+}$ transient (fig. S3A), although the contraction amplitude decreased due to the higher load (fig. S3B). Blebbistatin treatment attenuated mechanochemotransduction and restored the $Ca^{2+}$ transient to the load-free condition (fig. S3A). Therefore, afterload on cardiomyocytes during contraction increases the systolic $Ca^{2+}$ transient, which enhances contractility to counter mechanical load, but also leads to spontaneous $Ca^{2+}$ sparks during diastole, which are proarrhythmic. In the experiments below, we used the cell-in-gel system with Gel 7.5% to impose mechanical afterload during cardiomyocyte contraction.

Diastolic $Ca^{2+}$ sparks were few during the initial several beats of contraction, but then increased in frequency during subsequent beats (Fig. 2, A and B). Upon cessation of pacing, the sparks disappeared almost immediately. The initial latency suggested a buildup process for mechanochemotransduction to activate the signaling pathways that lead to modulation of ryanodine receptor (RyR) activity and increase of $Ca^{2+}$ sparks. Such latency

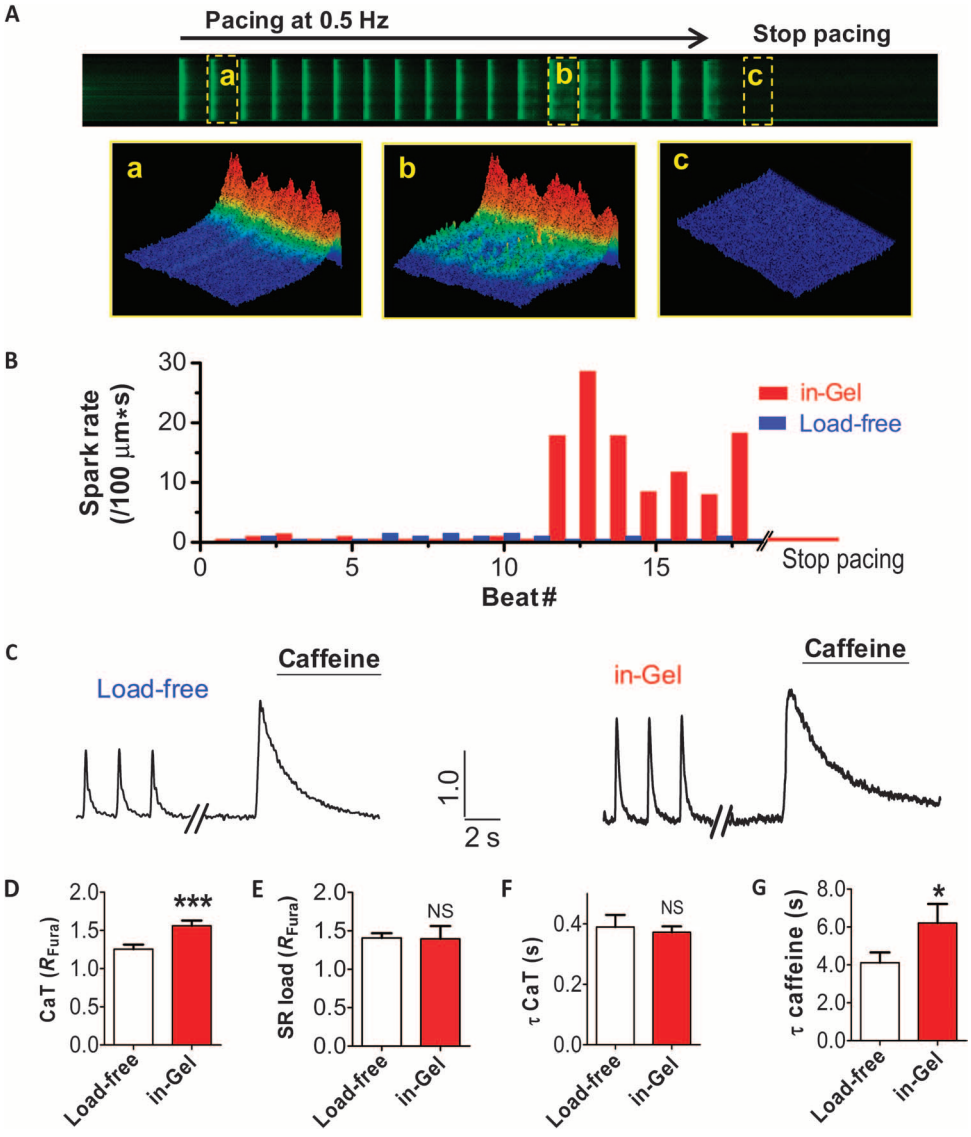


Fig. 2. Mechanochemotransduction and the SR load in contracting in-gel cardiomyocytes. $Ca^{2+}$ signaling in cardiomyocytes was monitored before, during, and after pacing to assess the temporal response of mechanochemotransduction. (**A**) Representative cardiomyocyte in-gel had very few $Ca^{2+}$ sparks before pacing; then, after an initial delay (a), it developed a large number of $Ca^{2+}$ sparks during paced contraction (b); when pacing stopped, the $Ca^{2+}$ sparks cleared out immediately (c). (**B**) $Ca^{2+}$ spark rate in a representative cardiomyocyte contracting in-gel compared to a load-free cardiomyocyte during the pacing protocol. Similar data were obtained from 20 in-gel cells and 12 load-free cells. (**C**) Representative recordings of the $Ca^{2+}$ transient (CaT) in a cardiomyocyte under load-free or in-gel contraction measured using Fura-2 ratio ($R_{fura}$). Scale bar: $R = 0.5$, $t = 2$ s. (**D**) The peak systolic $Ca^{2+}$ transient is higher in-gel ($n = 29$ cells) than load-free ($n = 19$). (**E**) The SR content was measured by applying caffeine 15 s after pacing was stopped to rapidly release $Ca^{2+}$ from SR. The SR content was similar for in-gel ($n = 9$) or load-free ($n = 17$) cardiomyocytes. NS, not significant. (**F**) τ of $Ca^{2+}$ transient was not different for in-gel ($n = 29$ cells) or load-free ($n = 19$) cardiomyocytes. (**G**) τ of the caffeine-induced decrease in $Ca^{2+}$ transient was higher for in-gel cardiomyocytes ($n = 9$) than for load-free cardiomyocytes ($n = 17$). Unpaired Student's *t* test; $^*P < 0.05$, $^{***}P < 0.001$.

agrees with a slow onset of the Anrep effect, which takes minutes to develop at the tissue level (*3*). The disappearance of $Ca^{2+}$ sparks after cessation of pacing is also consistent with a reversible effect of NO signaling (*15*, *16*).

To test whether the increase of $Ca^{2+}$ transient and $Ca^{2+}$ spark rate could be due to increased sarcoplasmic reticulum (SR) $Ca^{2+}$ content, we measured the cytosolic $Ca^{2+}$ concentration and SR content using a Fura-2 ratiometric method. The cardiomyocyte was paced at 0.5 Hz; after reaching steady state, pacing was stopped and caffeine (20 mM) was applied to rapidly release the SR $Ca^{2+}$ content (Fig. 2C). Although the systolic $Ca^{2+}$ transient was increased in the in-gel contracting cardiomyocytes compared to the load-free cardiomyocytes (Fig. 2D), the SR $Ca^{2+}$ content did not show detectable changes (Fig. 2E). Thus, the fractional SR $Ca^{2+}$ release was higher for the cardiomyocytes contracting in-gel, suggesting an increase in RyR sensitivity. Increased RyR sensitivity could also explain the increase of diastolic $Ca^{2+}$ sparks. High RyR sensitivity and diastolic SR $Ca^{2+}$ leak would reduce SR $Ca^{2+}$ content (*17*), unless it was compensated for by enhanced SR $Ca^{2+}$ uptake through the SR $Ca^{2+}$ adenosine triphosphatase (ATPase) (SERCA) or reduced $Ca^{2+}$ efflux through the $Na^+/Ca^{2+}$ exchanger. Indeed, the decline in systolic $Ca^{2+}$ transient was unaltered (Fig. 2F and fig. S4B), indicating that SR $Ca^{2+}$ uptake can reduce the intracellular $Ca^{2+}$ concentration despite greater release. Moreover, in-gel cardiomyocytes showed a slower decline of the caffeine-induced $Ca^{2+}$ transient (Fig. 2G), indicating that the $Ca^{2+}$ efflux through the $Na^+/Ca^{2+}$ exchanger and the sarcolemma $Ca^{2+}$ pump was reduced. These changes allow cardiomyocytes to maintain normal SR $Ca^{2+}$ content despite increased SR $Ca^{2+}$ release.

## Localized nNOS and eNOS signaling in mechanochemotransduction

We next examined whether nitric oxide signaling played a role in mediating afterload-induced changes in $Ca^{2+}$ handling. Cardiomyocytes were paced at 0.5 Hz until contraction reached steady state. In-gel cardiomyocytes displayed a high spontaneous $Ca^{2+}$ spark rate (Fig. 3, A and B). The general NOS inhibitor L-NAME ($N^G$-nitro-L-arginine methyl ester) effectively suppressed $Ca^{2+}$ sparks (Fig. 3B), indicating that NOS signaling is essential for mechanochemotransduction. Next, we assessed the contributions of the neuronal isoform (nNOS or NOS1) and the endothelial isoform (eNOS or NOS3) of NOS, both of which are constitutively expressed ventricular myocytes (*18*). $Ca^{2+}$ sparks were not suppressed by inhibition of eNOS with L-Nio-dihydrochloride (L-Nio) (Fig. 3, A and B), but were suppressed by inhibition of nNOS using $N^{\omega}$-propyl-L-arginine

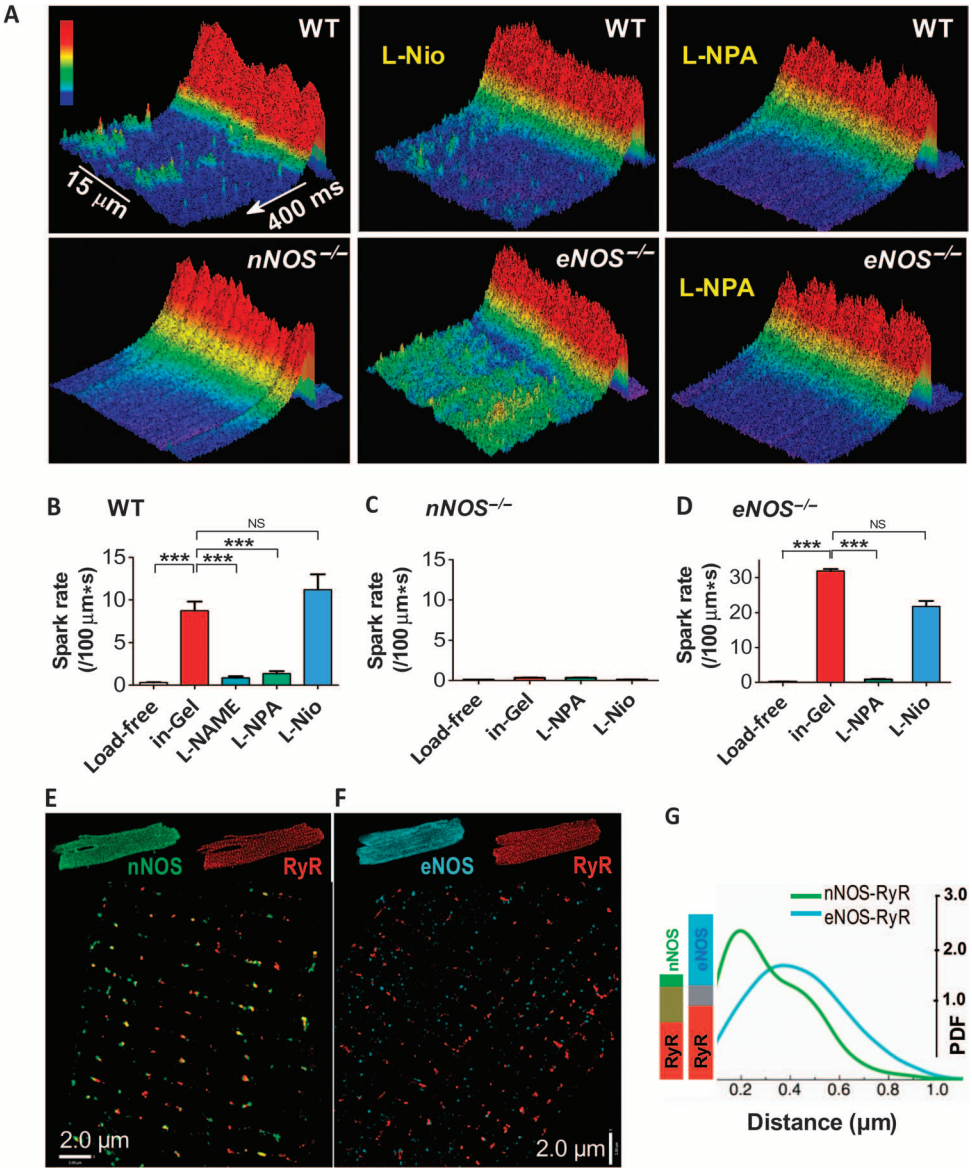


**Fig. 3. Differential role for nNOS and eNOS in mechanochemotransduction.** All data shown are from a cardiomyocyte contracting in-gel unless labeled Load-free. (**A**) The $Ca^{2+}$ transient and spontaneous $Ca^{2+}$ sparks seen in the 3D display of confocal linescan images of representative cardiomyocytes, obtained using Fluo-4 confocal imaging. (**B**) Mean ± SEM values of $Ca^{2+}$ spark rate in wild-type (WT) cardiomyocytes under load-free conditions ($n$ = 18 cells), in-gel ($n$ = 18), and treated with L-NAME ($n$ = 9), L-NPA ($n$ = 9), or L-Nio ($n$ = 10), respectively. (**C**) The $Ca^{2+}$ spark rate in *nNOS*$^{-/-}$ cardiomyocytes: $n$ = 8, 10, 10, and 9 cells for each group from left to right, respectively. (**D**) The $Ca^{2+}$ spark rate in *eNOS*$^{-/-}$ cardiomyocytes: $n$ = 10, 13, 6, and 6 cells for each group from left to right, respectively. One-way ANOVA with Bonferroni posttest was used for pairwise comparison; ***$P$ < 0.001. (**E** and **F**) Representative SIM images of nNOS-RyR (E) and eNOS-RyR (F); $n$ = 5 for each group. (**G**) Colocalization of nNOS-RyR and eNOS-RyR is depicted as the overlapping voxel volume (bars). Intermolecular distance histogram shows the probability density function (PDF) of the nearest-neighbor distance (curves). The kink in the curve for nNOS-RyR distance indicates that there is more than one population for nNOS-RyR distances. The Mann-Whitney test was used to compare the nNOS-RyR and the eNOS-RyR distance histograms, and the difference was significant at $P$ < 0.0001.

hydrochloride (L-NPA) (Fig. 3, A and B). These data suggest that nNOS, but not eNOS, mediates afterload-induced spontaneous $Ca^{2+}$ sparks. Furthermore, inhibition of nNOS with L-NPA did not affect the $Ca^{2+}$ transient (fig. S4A), whereas inhibition of eNOS with L-Nio not only reduced the peak $Ca^{2+}$ transient (fig. S4A) but also slowed the rate of the $Ca^{2+}$ transient decline (fig. S4B). These data suggest differential effects of nNOS and eNOS in modulating different $Ca^{2+}$ handling pathways.

Inhibition of nNOS and eNOS also reduced cardiomyocyte contraction (fig. S4C), in accordance to their effects on reducing the $Ca^{2+}$ transient. Interpretation of the contraction data needs to take into account the following complexity. When the cardiomyocyte is pulling mechanical load, the contraction amplitude is expected to decrease. However, without the mechanochemotransduction-mediated increase of $Ca^{2+}$ transient, the decrease in contraction would be more pronounced. That is, if the cardiomyocyte was purely elastic, the contraction would be less than that measured in a live cardiomyocyte with active mechanochemotransduction regulation to increase the $Ca^{2+}$ transient. To address this issue, we have performed mechanical analysis assuming a purely elastic cell without mechanochemotransduction (*14*). The knockdown factor, or the ratio of the cardiomyocyte shortening in-gel to that in load-free condition, is calculated to have a basal value of 0.2 for the elastic cell (*14*). However, the experimentally measured knockdown factor was 0.4 for the cardiomyocytes (fig. S4C); hence, the mechanochemotransduction-mediated increase in $Ca^{2+}$ transient enhanced contractility. Inhibiting nNOS or eNOS disrupts mechanochemotransduction signaling and, thus, reduced knockdown factor toward the basal value (fig. S4C).

To rule out possible nonspecific effects of pharmacological inhibitors, we also conducted experiments using cardiomyocytes from *nNOS*$^{-/-}$ and *eNOS*$^{-/-}$ mice. The *nNOS*$^{-/-}$ cardiomyocytes showed few afterload-induced $Ca^{2+}$ sparks (Fig. 3, A and C). In contrast, *eNOS*$^{-/-}$ cardiomyocytes exhibited a high $Ca^{2+}$ spark rate during contraction in-gel (Fig. 3, A and D), which was suppressed by inhibiting nNOS (Fig. 3, A and D). Therefore, nNOS, not eNOS, mediates the afterload-induced spontaneous $Ca^{2+}$ sparks.

Because NO is a short-lived local signaling molecule, the selective effect of nNOS compared to eNOS on $Ca^{2+}$ sparks could be explained if nNOS is physically closer than eNOS to RyR. In cardiomyocytes,

eNOS has been localized to caveolae (*19*), and nNOS has been localized at the SR (*20*) and also sarcolemma (*21*). For example, nNOS associates with various molecules at different subcellular locales, including SERCA in the SR membrane (*22*), the plasma membrane $Ca^{2+}$ ATPase (PMCA) in caveolae (*20*), and the structural protein dystrophin near the sarcolemma and t-tubules (*23*). The intermolecular distance of RyR to nNOS or eNOS had not been measured. Because confocal resolution cannot resolve these distances (fig. S5), we used super-resolution structured illumination microscopy (SIM) to quantify the colocalization of RyR with nNOS and eNOS. SIM images showed that nNOS was closely colocalized with RyR (Fig. 3E and movie S2), whereas eNOS was located farther from RyR (Fig. 3F and movie S3). Colocalization analyses yielded an overlap coefficient of 0.438 for nNOS-RyR and 0.125 for eNOS-RyR (Fig. 3G). The nearest-neighbor distance histogram (Fig. 3G) also showed significantly different patterns, with nNOS-RyR distance peaking at 0.19 μm and eNOS-RyR distance at 0.37 μm, a two-fold increase. The effective NO signaling range is expected to be influenced by the distance of diffusion, the amount of NO produced by NOS, the buffering capacity, the degradation and removal, and the target modification kinetics. The twofold increase in signaling distance would translate to four-fold slower diffusion time and eightfold reduction in NO concentration at the target site. Together, the above data suggest that the effective range of intracrine NO signaling in cardiomyocytes could be highly localized to within submicrometer distances.

## Mechanochemotransduction in cardiomyocytes from a cardiomyopathy model

To further explore the relationship between mechanical stress and $Ca^{2+}$ dynamics, we investigated cardiomyocytes from a mouse model of familial hypertrophic cardiomyopathy with R92Q mutation in cardiac troponin T. The R92Q mutation in human or mouse hearts causes increased myofilament $Ca^{2+}$ sensitivity and is associated with arrhythmias and sudden cardiac death (*24*–*28*). An unresolved question is how mutations in contractile proteins lead to arrhythmias (*29*, *30*). We found that the afterload-induced spontaneous $Ca^{2+}$ spark rate was significantly higher in R92Q cardiomyocytes (Fig. 4, A and B) than in wild-type cardiomyocytes (Fig. 4B). Consistently, the sparks were suppressed by inhibiting nNOS, but not eNOS (Fig. 4, A and B). Our data suggest that increased sensitivity in mechanochemotransduction leads to increased spontaneous $Ca^{2+}$ spark rate, and thus provide a possible explanation for $Ca^{2+}$-induced arrhythmogenesis in hearts from individuals with familial hypertrophic cardiomyopathy caused by the R92Q mutation (*31*–*34*).

## Role of NOX2 and CaMKII in afterload-induced mechanochemotransduction

We further tested whether NOX2-ROS signaling, which is activated by preload (*8*), might also be engaged by afterload. Inhibition of NOX2 using a specific peptide inhibitor gp91ds-tat decreased afterload-induced $Ca^{2+}$ sparks in wild-type, but not in R92Q, cardiomyocytes (Fig. 4B), suggesting that mechanochemotransduction differentially activated NOX2 and nNOS pathways in different models. Because NOX2 can be activated by nNOS signaling (*35*), a complex interplay between the two is expected, a result that warrants further investigation.

Because CaMKII can phosphorylate RyR to stimulate $Ca^{2+}$ sparks (*36*), we investigated the effect of CaMKII inhibition and found that the

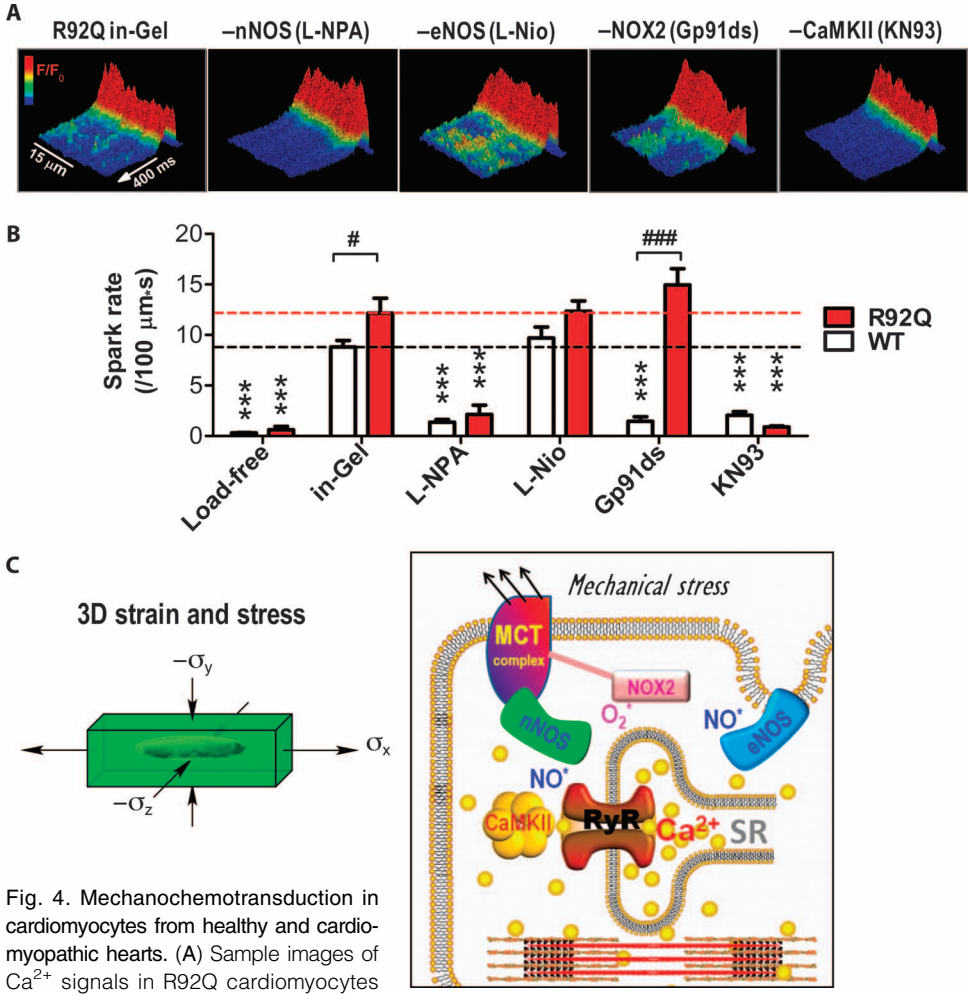


Fig. 4. Mechanochemotransduction in cardiomyocytes from healthy and cardiomyopathic hearts. (**A**) Sample images of $Ca^{2+}$ signals in R92Q cardiomyocytes during pacing at 1 Hz at body temperature, and the effect of inhibiting NOS isoforms, NOX2, and CaMKII. (**B**) The $Ca^{2+}$ spark rate in WT and R92Q cardiomyocytes. WT: load-free ($n$ = 18 cells), cell-in-gel ($n$ = 47), and cell-in-gel treated with L-NPA ($n$ = 9), L-Nio ($n$ = 9), Gp91ds ($n$ = 31), or KN93 ($n$ = 10). R92Q: load-free ($n$ = 12), cell-in-gel ($n$ = 20), and cell-in-gel treated with L-NPA ($n$ = 32), L-Nio ($n$ = 12), Gp91ds ($n$ = 16), or KN93 ($n$ = 23). Two-way ANOVA test shows significant difference in the spontaneous $Ca^{2+}$ spark rate between the R92Q and WT ($P < 0.0001$), significant drug effects ($P < 0.0001$), and also significant interaction ($P < 0.0001$). Bonferroni posttest shows significant difference for the drug effect compared to cell-in-gel without drug ($^{***}P < 0.001$) on each genotype; significantly higher spark rate in R92Q cardiomyocytes than in WT cardiomyocytes for cell-in-gel condition ($^{\#}P < 0.05$) and for Gp91ds effect ($^{\#\#\#}P < 0.001$) is also shown. (**C**) Schematic of the mechanochemotransduction pathway.

CaMKII blocker KN93 prevented the afterload-induced $Ca^{2+}$ sparks in cardiomyocytes from both wild-type and R92Q mice (Fig. 4B). To further investigate whether NO can activate CaMKII, we used the fluorescence resonance energy transfer (FRET)–based biosensor Camui (*37*) to measure the CaMKII activation induced by the NO donor SNAP. In human embryonic kidney cells expressing Camui, treatment with high, but not low, concentrations of SNAP increased CaMKII activation (as indicated by reduced FRET) in the presence of EGTA (fig. S6). CaMKII is autonomously activated by phosphorylation of $Thr^{286}$ (*38*) and by oxidation of $Cys^{280}/Met^{281}$ (*39*). To test whether one or both of these mechanisms were responsible for SNAP-induced activation of CaMKII, we assessed the effect of SNAP on mutant versions of Camui lacking either the phosphorylation ($Thr^{286}$) or oxidation ($Cys^{280}/Met^{281}$) target sites. In both cases, SNAP-dependent activation of CaMKII was preserved (fig. S6). These data indicate that CaMKII is subject to NO-induced activation that is independent of previously described phosphorylation and oxidation pathways.

## DISCUSSION

Using a cell-in-gel system, we have identified key molecules involved in mechanochemotransduction that respond to the mechanical load during cardiomyocyte contraction to regulate $Ca^{2+}$ handling. The systolic $Ca^{2+}$ transient is increased by afterload, which contributes to the Anrep effect (*3*, *4*, *40*, *41*). Both NOS isoforms were involved in increasing the $Ca^{2+}$ transient; however, the afterload-induced spontaneous $Ca^{2+}$ sparks were mediated by nNOS, but not eNOS. The divergent effects of nNOS and eNOS on modulating RyR might be explained by highly localized NO signaling; super-resolution imaging data suggested that the intracrine NO signaling was within submicrometer range in the cardiomyocytes. Our working hypothesis is that nNOS might predominantly modulate RyR and SERCA because of its closer proximity to the SR, whereas eNOS might predominantly affect the $Ca^{2+}$ handling proteins near the sarcolemma including $Na^{+}/Ca^{2+}$ exchange, sarcolemma $Ca^{2+}$ pump, and L-type $Ca^{2+}$ channels. In addition to NOS, CaMKII and NOX2 were also involved in afterload-associated mechanochemotransduction during cardiomyocyte contraction. Furthermore, we found that selective inhibition of nNOS and CaMKII suppressed afterload-induced spontaneous $Ca^{2+}$ activities in a model of familial hypertrophic cardiomyopathy, which is associated with a high incidence of cardiac arrhythmias (*28*, *42*, *43*). Hence, the mechano–NOS-CaMKII pathways we described here provide a working model (Fig. 4C) that, in combination with other pathways involving NOX (*8*), angiotensin II (*44*), transient receptor potential canonical channels (*45*), and others [review by (*4*)], help in understanding the mechanical stress effects on the heart. Mechanochemotransduction through NOS and CaMKII signaling pathways suggests novel points of therapeutic intervention for treating mechanical stress–induced $Ca^{2+}$ dysregulation, arrhythmias, and cardiomyopathy.

## MATERIALS AND METHODS

All laboratory procedures conform to the *Guide for the Care and Use of Laboratory Animals* published by the U.S. National Institutes of Health. Animal usage was approved by the local Institutional Animal Care and Use Committee.

### Cell isolation

Wild-type and transgenic mice were purchased from The Jackson Laboratory: C57BL/6J (wild type), B6.129S4-Nos1tm1Plh/J ($NOS1^{-/-}$), and B6.129P2-Nos3tm1Unc/J ($NOS3^{-/-}$). Transgenic mouse with R92Q mutation in cardiac troponin T was created in Tardiff's laboratory (*25*) and bred in Chen-Izu's laboratory. All mice used in the experiments were 12 to 18 weeks old and male. A standard enzymatic technique (*46*) was used to isolate the ventricular myocytes using Worthington collagenase type II and Sigma protease type XIV. All experiments were conducted at 21° to 22°C.

### Cell-in-gel system

Elastic gel matrix was made of a PVA hydrogel system composed of underivatized PVA (98 kD) and a tetravalent boronate-PEG cross-linker (*12*). Freshly isolated cardiomyocytes were first suspended in 7% PVA solution; then, 7.5% cross-linker solution was added in equal volume. Upon mixing, the boronate group cross-links PVA hydrogel, embedding the cell in the 3D gel matrix. The boronate group also cross-links the cis-diols of the cell surface glycans to PVA, thereby tethering the cell surface to the gel. We used the above gel made of 7.5% cross-linker (Gel 7.5%) for all the experiments in this study, except for one group in Fig. 1G, wherein we used a softer gel made of 5% cross-linker (Gel 5%). To rule out that the gel alone might affect $Ca^{2+}$ signaling, we examined the $Ca^{2+}$ signals in the in-gel cardiomyocytes at resting state; the data showed no spontaneous $Ca^{2+}$ activity in resting cells before or after paced contraction (Fig. 2A). To examine whether individual gel component might affect cardiomyocytes, we preincubated rabbit ventricular myocytes with PVA or cross-linker alone, followed by perfusion with the normal Tyrode solution and contraction measurement; neither PVA nor cross-linker treatment had any effect on contraction measured as fractional shortening (fig. S2).

### Confocal imaging of $Ca^{2+}$ signals

Confocal imaging of the Fluo-4 signals was primarily used to detect the $Ca^{2+}$ sparks and waves, because Fluo-4 is among the most sensitive indicators for detecting small changes in the local $Ca^{2+}$ signals owning to its high quantum yield. Cardiomyocytes were loaded with the $Ca^{2+}$ indicator Fluo-4 and then embedded in the gel. Confocal imaging was performed with standard methods (*47*) with an Olympus FluoView FV1000 confocal microscope (inverted configuration) with a water immersion fluorescence objective UPlanSApo 60×, 1.2 numerical aperture (NA) (corrected for the thickness of the no. 1 glass coverslip that is used at the bottom of the perfusion chamber). Fluo-4 was excited with a 488-nm laser beam (laser power set to 5%), and the emitted fluorescence light was passed through a bandpass filter BA505-605 and collected with a photon multiplier tube (PMT). The PMT voltage, gain, and offset were set to avoid any saturation and to obtain high-fidelity images. The linescan images were obtained using the highest scan speed of 2 μs per pixel.

$Ca^{2+}$ sparks were detected automatically using a custom program based on our spark identification algorithm and adapted for *x-t* linescan images (*48*). Sparks were identified in two stages. In the first stage, putative sparks are detected on the basis of Cheng *et al.*'s description (*49*), and bright but spatially small events were eliminated using our previously described "live-or-die" algorithm (*50*). In the second stage, the putative sparks were classified as sparks or noise on the basis of the statistical sieve as described in our previous publication (*48*). This analysis software provides automated and objective (agnostic through statistical sieving) detection and classification of the $Ca^{2+}$ signaling events in confocal linescan images.

### Fura-2 ratiometric measurement of $Ca^{2+}$ concentration

To measure the intracellular $Ca^{2+}$ concentration, we used Fura-2 dual-wavelength ratiometric method (*46*), which is more precise than using the Fluo-4 single-wavelength method. Isolated cardiomyocytes were continuously perfused in Tyrode solution containing 150 mM NaCl, 5.4 mM KCl, 1.2 mM $MgCl_2$, 1 mM $CaCl_2$, at pH 7.4, incubated with 2.5 μM Fura-2/acetoxymethyl (AM) and 0.75 μM Pluronic F127 (in 20% dimethyl sulfoxide) at room temperature for 30 min, washed, embedded in the PVA

gel, and used for experiments within 2 hours. Cells were paced at 0.5-Hz frequency by electrical field stimulation using short (4 ms) depolarization pulses with bipolar switching (switch positive and negative polarity in consecutive stimulus pulses) applied with a pair of platinum electrodes. Continuous perfusion of fresh Tyrode solution was used to maintain constant bath conditions (pH, glucose, ionic composition, temperature, and so on). An IonOptix system (IonOptix Inc.) with a HyperSwitch was mounted on the Olympus X71 inverted microscope with a water immersion fluorescence objective UPlanSApo 40×, 1.15 NA (corrected for the thickness of the no. 1 glass coverslip used as the bottom of the chamber). The excitation light was generated using a high-intensity arc lamp (Cairn). The galvanometer-based HyperSwitch delivered dual-excitation beams at 340 and 380 nm using a 340/370d/380 filter cube, switching between the two wavelengths at a frequency of 500 Hz. Fura-2 fluorescence emission light was passed through a bandpass filter D510/40m and collected in a PMT. The background fluorescence signals at 340- and 380-nm channels were obtained in both the Tyrode solution and the gel without cells; the background signals were slightly higher in the gel than in the solution, but substantially lower than the Fura-2 fluorescence emissions from cells. The Fura-2 fluorescence ratio, $R_{Fura}$, was calculated from the fluorescence emissions from cells at 340- and 380-nm excitation wavelengths after background subtraction.

For measuring systolic $Ca^{2+}$ transient, the cell was first paced to reach steady state (>2 min), and then Fura-2 fluorescence was recorded for at least 10 beats during steady state. For SR content measurement, after the cell reached steady state, field stimulation was stopped to keep the cell at a resting state for 15 s; then, caffeine at high concentration (20 mM) was applied to rapidly deplete the SR load. The rapidity of the SR $Ca^{2+}$ release was accessed by the rising velocity of the caffeine-induced $Ca^{2+}$ transient, and the peak $Ca^{2+}$ value was used as an index to measure the SR load. As noted, the SR $Ca^{2+}$ content measured using either Fura-2 (Fig. 2E) or Fluo-4 did not show any discernible difference between the cell-in-gel and the load-free contraction. Because RyR sensitivity to the intra-SR $Ca^{2+}$ concentration is steep, we also acknowledge that small changes in SR $Ca^{2+}$ content below the precision of the Fura-2 method could have a functional impact.

## Structured illumination microscopy

We used a DeltaVision OMX V3.0 Blaze system (Applied Precision Inc.) to acquire the fluorescence images of antibody-labeled cardiomyocytes as previously described (*51*). Briefly, the system uses 488- and 532-nm lasers as the light source for illumination. A grating in the beam path generated three coherent beams that created 3D structured illumination patterns in the sample. The antibody-labeled cells were immersed in the ProLong Gold antifade reagent with 1.47 refractive index (RI), and fluorescence emission was collected with a 60× oil immersion objective with 1.514 RI, 1.42 NA. Fluorescence of different colors was separated by a dichroic mirror and filtered by bandpass emission filters before being collected by two fast sCMOS cameras (PCO-TECH Inc.). To acquire 3D images, the sample was moved along the *z* direction at a step size of 125 nm. For each slice, the illumination pattern was rotated three times and shifted five times, resulting in a total of 15 exposures per channel. Acquired raw images were processed with a proprietary software package (softWoRx v5.0, Applied Precision Inc.) to reconstruct super-resolution 3D images. Reconstructed images of different colors were registered using custom-built software to correct chromatic aberrations and image distortions. Before the experiments, the system and the color registration software were calibrated using multicolor polymeric beads of 0.1 μm (TetraSpeck beads, Molecular Probes). The spatial resolution of the system was ~110 nm for the *x* and *y* axes and ~250 nm for the *z* axis. The color registration error was smaller than a pixel (namely, 40 nm). 3D rendering of the SIM images was performed with Volocity Visualization package.

The colocalization of nNOS or eNOS with RyR was analyzed using Volocity Quantitation (PerkinElmer), implementing the standard Pearson's colocalization analysis (*52*). A user-defined threshold was set to separate signal from background, and Mander's overlapping coefficients (M1 and M2) were calculated (*51*). The extent of colocalization was measured by M1and M2 values depicted by the overlapping regions (mixed color in the bars) in Fig. 3G. The bars represent the voxel volume of nNOS (green)–RyR (red) and eNOS (cyan)–RyR (red), each normalized to the RyR voxel volume. Note that M1 and M2 values give a general measure of colocalization, but do not quantify the physical distances between molecules.

The nearest-neighbor distance between NOS and RyR clusters was measured as the smallest pairwise distance between the center of mass of the respective molecular clusters (*51*). Objects (blobs) having a volume smaller than 0.00189 $\mu m^3$ (which might arise from photon noise) were excluded in the pairwise distance calculations. The center of mass and the nearest-neighbor distances were determined using the Volocity Quantitation software package.

## Confocal imaging of antibody-labeled cells

Confocal images were obtained using an Olympus FluoView FV1000 confocal microscope (inverted configuration) with a water immersion fluorescence objective UPlanSApo 60×, 1.2 NA (corrected for the thickness of the no. 1 glass coverslip used at the bottom of the chamber). The water immersion objective was used to match the RI of the solution in which the cells are kept to minimize spherical aberration. The confocal aperture was set to 1 airy unit to obtain the thinnest optical sectioning for highest spatial resolution. The confocal images were acquired using 2D scan. For imaging dual labeled cells, the "sequential mode" was used to switch between the two excitation beams to minimize crosstalk between the spectra of the two different fluorophores. The emitted fluorescence lights were separated by dichroic mirror into two channels and passed through corresponding bandpass filters (BA505-525 for green and BA560-660 for red colors), and then collected with a PMT for each channel. The highest spatial resolution of the confocal images was ~0.3 μm at the *x* and *y* axes, and 0.8 to 1 μm at the *z* axis.

## Cardiomyocyte contraction measurement

We used the IonOptix sarcomere detection and fast Fourier transform (FFT) method rather than Fluo-4 confocal imaging edge detection to measure cardiomyocyte contraction because the latter may lose precision if the cell's ends move out of the focal plane during contraction. Contraction was measured using an IonOptix system (IonOptix Co.) with a high-speed camera (MyoCam-S, 240 to 1000 frames/s) to record sarcomere movement during cardiomyocyte contraction. The sarcomere pattern was then used to calculate the sarcomere length using an FFT algorithm. The fractional shortening was then calculated as the percentage of change in sarcomere length during contraction.

## Statistical tests

The numerical values are calculated for the mean, SD, and SEM. Mean ± SEM values are shown in the bar charts in all figures. The number of cells in each experimental group was reported in the figure captions, and the cells in each group came from three to six individual animals. Given the biological variability among cells, each cell was treated as independent in the statistical tests, although multiple cells may come from one animal. For data with a normal distribution, Student's *t* test (unpaired, unequal variance) was used to compare two different groups. One-way ANOVA was used to compare multiple groups, and a Bonferroni posttest was used for pairwise comparisons. Two-way ANOVA was used to compare multiple groups with

two distinct factors, with Bonferroni posttest for pairwise comparisons. For data with a nonnormal distribution, such as the nNOS-RyR and eNOS-RyR distance histograms in Fig. 3C, the Mann-Whitney test was used to compare between two groups. The difference was deemed significant if $P < 0.05$, and denoted $*P < 0.05$, $**P < 0.01$, and $***P < 0.001$. All statistical tests were performed with GraphPad Prism Software (http://www.graphpad.com/).

## SUPPLEMENTARY MATERIALS

www.sciencesignaling.org/cgi/content/full/7/317/ra27/DC1
Materials and Methods
Fig. S1. PVA–cross-linker system for embedding single cardiomyocytes in a 3D elastic matrix.
Fig. S2. PVA or cross-linker alone did not affect contraction.
Fig. S3. Mechanical stress effects on the systolic $Ca^{2+}$ transient and contraction.
Fig. S4. Effect of inhibiting nNOS or eNOS on cardiomyocytes.
Fig. S5. Distribution of RyR, nNOS, and eNOS in a wild-type cardiomyocyte.
Fig. S6. NO-dependent activation of CaMKII.
Movie S1. Cell-in-gel contraction.
Movie S2. 3D rendition of nNOS-RyR colocalization.
Movie S3. 3D rendition of eNOS-RyR distribution.

## REFERENCES AND NOTES


1. G. von Anrep, On the part played by the suprarenals in the normal vascular reactions of the body. *J. Physiol.* **45**, 307–317 (1912).
2. S. J. Sarnoff, J. H. Mitchell, J. P. Gilmore, J. P. Remensnyder, Homeometric autoregulation in the heart. *Circ. Res.* **8**, 1077–1091 (1960).
3. C. G. Nichols, D. A. Hanck, B. R. Jewell, The Anrep effect: An intrinsic myocardial mechanism. *Can. J. Physiol. Pharmacol.* **66**, 924–929 (1988).
4. H. E. Cingolani, N. G. Pérez, O. H. Cingolani, I. L. Ennis, The Anrep effect: 100 years later. *Am. J. Physiol. Heart Circ. Physiol.* **304**, H175–H182 (2013).
5. H. E. ter Keurs, Heart failure and Starling's law of the heart. *Can. J. Cardiol.* **12**, 1047–1057 (1996).
6. M. G. Petroff, S. H. Kim, S. Pepe, C. Dessy, E. Marbán, J. L. Balligand, S. J. Sollott, Endogenous nitric oxide mechanisms mediate the stretch dependence of $Ca^{2+}$ release in cardiomyocytes. *Nat. Cell Biol.* **3**, 867–873 (2001).
7. B. L. Prosser, C. W. Ward, W. J. Lederer, Subcellular $Ca^{2+}$ signaling in the heart: The role of ryanodine receptor sensitivity. *J. Gen. Physiol.* **136**, 135–142 (2010).
8. B. L. Prosser, C. W. Ward, W. J. Lederer, X-ROS signaling: Rapid mechano-chemo transduction in heart. *Science* **333**, 1440–1445 (2011).
9. J. A. Chirinos, P. Segers, Noninvasive evaluation of left ventricular afterload: Part 2: Arterial pressure-flow and pressure-volume relations in humans. *Hypertension* **56**, 563–570 (2010).
10. K. Toischer, A. G. Rokita, B. Unsöld, W. Zhu, G. Kararigas, S. Sossalla, S. P. Reuter, A. Becker, N. Teucher, T. Seidler, C. Grebe, L. Preub, S. N. Gupta, K. Schmidt, S. E. Lehnart, M. Krüger, W. A. Linke, J. Backs, V. Regitz-Zagrosek, K. Schäfer, L. J. Field, L. S. Maier, G. Hasenfuss, Differential cardiac remodeling in preload versus afterload. *Circulation* **122**, 993–1003 (2010).
11. S. H. Shin, C. L. Hung, H. Uno, A. H. Hassanein, A. Verma, M. Bourgoun, L. Køber, J. K. Ghali, E. J. Velazquez, R. M. Califf, M. A. Pfeffer, S. D. Solomon; Valsartan in Acute Myocardial Infarction Trial (VALIANT) Investigators, Mechanical dyssynchrony after myocardial infarction in patients with left ventricular dysfunction, heart failure, or both. *Circulation* **121**, 1096–1103 (2010).
12. E. Onofiok, K. S. Lam, J. Luo, Three dimensional cell adhesion matrix, Patent WO/2010/148346 (2010).
13. D. J. Grieve, J. A. Byrne, A. Siva, J. Layland, S. Johar, A. C. Cave, A. M. Shah, Involvement of the nicotinamide adenosine dinucleotide phosphate oxidase isoform Nox2 in cardiac contractile dysfunction occurring in response to pressure overload. *J. Am. Coll. Cardiol.* **47**, 817–826 (2006).
14. J. Shaw, L. Izu, Y. Chen-Izu, Mechanical analysis of single myocyte contraction in a 3-D elastic matrix. *PLOS One* **8**, e75492 (2013).
15. D. Stoyanovsky, T. Murphy, P. R. Anno, Y. M. Kim, G. Salama, Nitric oxide activates skeletal and cardiac ryanodine receptors. *Cell Calcium* **21**, 19–29 (1997).
16. G. Lim, L. Venetucci, D. A. Eisner, B. Casadei, Does nitric oxide modulate cardiac ryanodine receptor function? Implications for excitation–contraction coupling. *Cardiovasc. Res.* **77**, 256–264 (2008).
17. D. A. Eisner, H. S. Choi, M. E. Díaz, S. C. O'Neill, A. W. Trafford, Integrative analysis of calcium cycling in cardiac muscle. *Circ. Res.* **87**, 1087–1094 (2000).
18. L. A. Barouch, R. W. Harrison, M. W. Skaf, G. O. Rosas, T. P. Cappola, Z. A. Kobeissi, I. A. Hobai, C. A. Lemmon, A. L. Burnett, B. O'Rourke, E. R. Rodriguez, P. L. Huang, J. A. C. Lima, D. E. Berkowitz, J. M. Hare, Nitric oxide regulates the heart by spatial confinement of nitric oxide synthase isoforms. *Nature* **416**, 337–339 (2002).
19. O. Feron, L. Belhassen, L. Kobzik, T. W. Smith, R. A. Kelly, T. Michel, Endothelial nitric oxide synthase targeting to caveolae. Specific interactions with caveolin isoforms in cardiac myocytes and endothelial cells. *J. Biol. Chem.* **271**, 22810–22814 (1996).
20. J. C. Williams, A. L. Armesilla, T. M. A. Mohamed, C. L. Hagarty, F. H. McIntyre, S. Schomburg, A. O. Zaki, D. Oceandy, E. J. Cartwright, M. H. Buch, M. Emerson, L. Neyses, The sarcolemmal calcium pump, α-1 syntrophin, and neuronal nitric-oxide synthase are parts of a macromolecular protein complex. *J. Biol. Chem.* **281**, 23341–23348 (2006).
21. T. M. A. Mohamed, D. Oceandy, M. Zi, S. Prehar, N. Alatwi, Y. Wang, M. A. Shaheen, R. Abou-Leisa, C. Schelcher, Z. Hegab, F. Baudoin, M. Emerson, M. Mamas, G. Di Benedetto, M. Zaccolo, M. Lei, E. J. Cartwright, L. Neyses, Plasma membrane calcium pump (PMCA4)-neuronal nitric-oxide synthase complex regulates cardiac contractility through modulation of a compartmentalized cyclic nucleotide microdomain. *J. Biol. Chem.* **286**, 41520–41529 (2011).
22. N. Burkard, A. G. Rokita, S. G. Kaufmann, M. Hallhuber, R. Wu, K. Hu, U. Hofmann, A. Bonz, S. Frantz, E. J. Cartwright, L. Neyses, L. S. Maier, S. K. G. Maier, T. Renné, K. Schuh, O. Ritter, Conditional neuronal nitric oxide synthase overexpression impairs myocardial contractility. *Circ. Res.* **100**, e32–e44 (2007).
23. Y. Lai, J. Zhao, Y. Yue, D. Duan, α2 and α3 helices of dystrophin R16 and R17 frame a microdomain in the α1 helix of dystrophin R17 for neuronal NOS binding. *Proc. Natl. Acad. Sci. U.S.A.* **110**, 525–530 (2013).
24. D. Szczesna, R. Zhang, J. Zhao, M. Jones, G. Guzman, J. D. Potter, Altered regulation of cardiac muscle contraction by troponin T mutations that cause familial hypertrophic cardiomyopathy. *J. Biol. Chem.* **275**, 624–630 (2000).
25. M. Chandra, V. L. Rundell, J. C. Tardiff, L. A. Leinwand, P. P. de Tombe, R. J. Solaro, $Ca^{2+}$ activation of myofilaments from transgenic mouse hearts expressing R92Q mutant cardiac troponin T. *Am. J. Physiol. Heart Circ. Physiol.* **280**, H705–H713 (2001).
26. F. Yanaga, S. Morimoto, I. Ohtsuki, $Ca^{2+}$ sensitization and potentiation of the maximum level of myofibrillar ATPase activity caused by mutations of troponin T found in familial hypertrophic cardiomyopathy. *J. Biol. Chem.* **274**, 8806–8812 (1999).
27. S. Morimoto, F. Yanaga, R. Minakami, I. Ohtsuki, $Ca^{2+}$-sensitizing effects of the mutations at Ile-79 and Arg-92 of troponin T in hypertrophic cardiomyopathy. *Am. J. Physiol.* **275**, C200–C207 (1998).
28. H. Watkins, W. J. McKenna, L. Thierfelder, H. J. Suk, R. Anan, A. O'Donoghue, P. Spirito, A. Matsumori, C. S. Moravec, J. G. Seidman, C. E. Seidman, Mutations in the genes for cardiac troponin T and α-tropomyosin in hypertrophic cardiomyopathy. *N. Engl. J. Med.* **332**, 1058–1064 (1995).
29. O. M. Hernandez, P. R. Housmans, J. D. Potter, Invited review: Pathophysiology of cardiac muscle contraction and relaxation as a result of alterations in thin filament regulation. *J. Appl. Physiol.* **90**, 1125–1136 (2001).
30. J. C. Tardiff, Sarcomeric proteins and familial hypertrophic cardiomyopathy: Linking mutations in structural proteins to complex cardiovascular phenotypes. *Heart Fail. Rev.* **10**, 237–248 (2005).
31. P. A. Boyden, C. Barbhaiya, T. Lee, H. E. ter Keurs, Nonuniform $Ca^{2+}$ transients in arrhythmogenic Purkinje cells that survive in the infarcted canine heart. *Cardiovasc. Res.* **57**, 681–693 (2003).
32. J. R. Berlin, M. B. Cannell, W. J. Lederer, Cellular origins of the transient inward current in cardiac myocytes. Role of fluctuations and waves of elevated intracellular calcium. *Circ. Res.* **65**, 115–126 (1989).
33. R. S. Kass, W. J. Lederer, R. W. Tsien, R. Weingart, Role of calcium ions in transient inward currents and aftercontractions induced by strophanthidin in cardiac Purkinje fibres. *J. Physiol.* **281**, 187–208 (1978).
34. G. R. Ferrier, G. K. Moe, Effect of calcium on acetylstrophanthidin-induced transient depolarizations in canine Purkinje tissue. *Circ. Res.* **33**, 508–515 (1973).
35. H. Girouard, G. Wang, E. F. Gallo, J. Anrather, P. Zhou, V. M. Pickel, C. Iadecola, NMDA receptor activation increases free radical production through nitric oxide and NOX2. *J. Neurosci.* **29**, 2545–2552 (2009).
36. T. Guo, T. Zhang, R. Mestril, D. M. Bers, $Ca^{2+}$/calmodulin-dependent protein kinase II phosphorylation of ryanodine receptor does affect calcium sparks in mouse ventricular myocytes. *Circ. Res.* **99**, 398–406 (2006).
37. J. R. Erickson, R. Patel, A. Ferguson, J. Bossuyt, D. M. Bers, Fluorescence resonance energy transfer–based sensor Camui provides new insight into mechanisms of calcium/calmodulin-dependent protein kinase II activation in intact cardiomyocytes. *Circ. Res.* **109**, 729–738 (2011).
38. L. L. Lou, S. J. Lloyd, H. Schulman, Activation of the multifunctional $Ca^{2+}$/calmodulin-dependent protein kinase by autophosphorylation: ATP modulates production of an autonomous enzyme. *Proc. Natl. Acad. Sci. U.S.A.* **83**, 9497–9501 (1986).
39. J. R. Erickson, M. I. A. Joiner, X. Guan, W. Kutschke, J. Yang, C. V. Oddis, R. K. Bartlett, J. S. Lowe, S. E. O'Donnell, N. Aykin-Burns, M. C. Zimmerman, K. Zimmerman, A. J. L. Ham, R. M. Weiss, D. R. Spitz, M. A. Shea, R. J. Colbran, P. J. Mohler, M. E. Anderson, A dynamic pathway for calcium-independent activation of CaMKII by methionine oxidation. *Cell* **133**, 462–474 (2008).

40. J. C. Kentish, A. Wrzosek, Changes in force and cytosolic $Ca^{2+}$ concentration after length changes in isolated rat ventricular trabeculae. *J. Physiol.* **506** (Pt. 2), 431–444 (1998).
41. B. V. Alvarez, N. G. Pérez, I. L. Ennis, M. C. Camilión de Hurtado, H. E. Cingolani, Mechanisms underlying the increase in force and $Ca^{2+}$ transient that follow stretch of cardiac muscle: A possible explanation of the Anrep effect. *Circ. Res.* **85**, 716–722 (1999).
42. J. C. Moolman, V. A. Corfield, B. Posen, K. Ngumbela, C. Seidman, P. A. Brink, H. Watkins, Sudden death due to troponin T mutations. *J. Am. Coll. Cardiol.* **29**, 549–555 (1997).
43. B. J. Maron, J. M. Gardin, J. M. Flack, S. S. Gidding, T. T. Kurosaki, D. E. Bild, Prevalence of hypertrophic cardiomyopathy in a general population of young adults. Echocardiographic analysis of 4111 subjects in the CARDIA Study. *Circulation* **92**, 785–789 (1995).
44. J. Kockskämper, D. von Lewinski, M. Khafaga, A. Elgner, M. Grimm, T. Eschenhagen, P. A. Gottlieb, F. Sachs, B. Pieske, The slow force response to stretch in atrial and ventricular myocardium from human heart: Functional relevance and subcellular mechanisms. *Prog. Biophys. Mol. Biol.* **97**, 250–267 (2008).
45. K. Seo, P. P. Rainer, D. l. Lee, S. Hao, D. Bedja, L. Birnbaumer, O. H. Cingolani, D. A. Kass, Hyperactive adverse mechanical-stress responses in dystrophic heart are coupled to TRPC6 and blocked by cGMP-PKG modulation. *Circ. Res.* **114**, 823–832 (2014).
46. Y. Chen-Izu, L. Chen, T. Bányász, S. L. McCulle, B. Norton, S. M. Scharf, A. Agarwal, A. R. Patwardhan, L. T. Izu, C. W. Balke, Hypertension-induced remodeling of cardiac excitation-contraction coupling in ventricular myocytes occurs prior to hypertrophy development. *Am. J. Physiol. Heart Circ. Physiol.* **293**, H3301–H3310 (2007).
47. M. M. Kirk, L. T. Izu, Y. Chen-Izu, S. L. McCulle, W. G. Wier, C. W. Balke, S. R. Shorofsky, Role of the transverse-axial tubule system in generating calcium sparks and calcium transients in rat atrial myocytes. *J. Physiol.* **547**, 441–451 (2003).
48. T. Bányász, Y. Chen-Izu, C. W. Balke, L. Izu, A new approach to the detection and classification of $Ca^{2+}$ sparks. *Biophys. J.* **92**, 4458–4465 (2007).
49. H. Cheng, L. S. Song, N. Shirokova, A. González, E. G. Lakatta, E. Ríos, M. D. Stern, Amplitude distribution of calcium sparks in confocal images: Theory and studies with an automatic detection method. *Biophys. J.* **76**, 606–617 (1999).
50. Y. Chen-Izu, S. L. McCulle, C. W. Ward, C. Soeller, B. M. Allen, C. Rabang, M. B. Cannell, C. W. Balke, L. T. Izu, Three-dimensional distribution of ryanodine receptor clusters in cardiac myocytes. *Biophys. J.* **91**, 1–13 (2006).
51. T. Zhang, S. Osborn, C. Brandow, D. Dwyre, R. Green, S. Lane, S. Wachsmann-Hogiu, Structured illumination-based super-resolution optical microscopy for hemato- and cytopathology applications. *Anal. Cell. Pathol.* **36**, 27–35 (2013).
52. A. L. Barlow, A. Macleod, S. Noppen, J. Sanderson, C. J. Guérin, Colocalization analysis in fluorescence micrographs: Verification of a more accurate calculation of Pearson's correlation coefficient. *Microsc. Microanal.* **16**, 710–724 (2010).

**Acknowledgments:** We thank W. J. Lederer (University of Maryland), R. Ross [University of California (UC), San Diego], and R. Moss (University of Wisconsin-Madison) for scientific discussions on mechanochemotransduction. **Funding:** This work was funded by NIH R03-AG031944 to Y.C.-I., R01-HL90880 to L.T.I. and Y.C.-I., R21-HL108300 to K.S.L., R37-HL30077 to D.M.B., and R01-HL075274 and R01-HL085844 and VA Merit Review Grant I01 BX000576 to N.C. H.H. and R.S. were supported, in part, by T32-HL86350 Training Grant (to N.C.). T.Z. and J.C. were supported by the Center for Biophotonics Science and Technology, a designated National Science Foundation Science and Technology Center managed by UC Davis, under Cooperative Agreement No. PHY0120999. This work was also supported, in part, by the UC Proof of Concept Grant #247525 to K.S.L. and Y.C.-I, and the UC Davis Startup funds to Y.C.-I. **Author contributions:** Project and experimental designs were done by Y.C.-I., K.S.L., L.T.I., J.C.T., T.B., N.C., and D.M.B. Chemical synthesis and purification were done by E.O., W.X., Y.L., and K.S.L. Transgenic mouse R92Q was provided by J.C.T. Experiments were performed by Z.J., H.H., T.Z., J.R.E., Y.-J.C., B.H., R.S., and Y.C.-I. Data analyses and statistical tests were performed by Z.J., H.H., T.Z., J.P., L.T.I., J.A.S., J.R.E., R.S., T.P., J.C., and Y.C.-I. Manuscript writing and editing were done by Y.C.-I., H.H., L.T.I., N.C., K.S.L., and D.M.B. **Competing interests:** The authors declare that they have no competing interests.

Submitted 3 January 2014
Accepted 28 February 2014
Final Publication 18 March 2014
10.1126/scisignal.2005046
**Citation:** Z. Jian, H. Han, T. Zhang, J. Puglisi, L. T. Izu, J. A. Shaw, E. Onofiok, J. R. Erickson, Y.-J. Chen, B. Horvath, R. Shimkunas, W. Xiao, Y. Li, T. Pan, J. Chan, T. Banyasz, J. C. Tardiff, N. Chiamvimonvat, D. M. Bers, K. S. Lam, Y. Chen-Izu, Mechanochemotransduction during cardiomyocyte contraction is mediated by localized nitric oxide signaling. *Sci. Signal.* **7**, ra27 (2014).

Science Signaling
AAAS

www.sciencesignaling.org/cgi/content/full/7/317/ra27/DC1

# Supplementary Materials for

## Mechanochemotransduction During Cardiomyocyte Contraction Is Mediated by Localized Nitric Oxide Signaling

Zhong Jian, Huilan Han, Tieqiao Zhang, Jose Puglisi, Leighton T. Izu, John A. Shaw, Ekama Onofiok, Jeffery R. Erickson, Yi-Je Chen, Balazs Horvath, Rafael Shimkunas, Wenwu Xiao, Yuanpei Li, Tingrui Pan, James Chan, Tamas Banyasz, Jil C. Tardiff, Nipavan Chiamvimonvat, Donald M. Bers, Kit S. Lam, Ye Chen-Izu*

*Corresponding author. E-mail: ychenizu@ucdavis.edu

Published 18 March 2014, *Sci. Signal.* **7**, ra27 (2014)
DOI: 10.1126/scisignal.2005046

**This PDF file includes:**



**Other Supplementary Material for this manuscript includes the following:**
(available at www.sciencesignaling.org/cgi/content/full/7/317/ra27/DC1)

# MATERIALS AND METHODS

**Mechanical analysis of cardiomyocyte contraction in 3D elastic matrix**

The stiffness of the PVA gel was measured using a TA-XT2 Texture Analyzer (Stable Micro Systems, England). PVA gel sample of 50 mm diameter and 1.5 mm thickness was submitted to a unidirectional strain. The applied strain of 10% was small enough to remain in the linear region of the stress-strain response, and the Young's modulus was calculated from the slope of stress versus strain plot. Unless indicated otherwise, experiments in this study were conducted using Gel7.5% with Young's modulus of 1 KPa.

**Antibody labeling of freshly isolated ventricular myocytes**

Antibody labeling of freshly isolated ventricular myocytes was done based on our previously described protocol [50] with minor modifications. Briefly, cells were washed in the normal phosphate buffer solution (PBS) at room temperature, and then fixed in 1% paraformaldehyde PBS solution for 10 minute. After being washed twice in cold PBS (on ice or in the refrigerator at 4$^{o}$C), the cells were then permeablized in cold 0.1% Triton X-100 PBS solution for 10 min. Cells were incubated with the primary antibody (1:100 dilution) solution containing 5% bovine serum albumin, 3% goat serum and 0.01% Triton X-100 in PBS for 2 hours at room temperature; washed twice in cold PBS, and then incubated with the secondary antibody (1:100 dilution, Molecular Probes, USA) solution for 2 hours at room temperature or overnight at 4$^{o}$C. For antibody labeling of RyR, nNOS, and eNOS, we used anti-RyR monoclonal antibody (clone C3-33, Affinity BioReagents Inc. USA), anti-nNOS polyclonal antibody (Thermo Scientific), and anti-eNOS polyclonal antibody (Thermo Scientific), respectively.

For colocalization studies, we labeled the cells with two primary antibodies from different species to simultaneously label molecule A and B (A/B pair) in the same cell; fluorophore-conjugated secondary antibodies targeting each of the primary antibodies were then used simultaneously to visualize A and B. The fluorophores were chosen to detect A and B in two separate emission channels with sufficient spectral separation. For example, nNOS was labeled with Alexa555-conjugated anti-rabbit IgG antibody, whereas RyR was labeled with Alexa488-conjugated anti-mouse IgG antibody. The 'Sequential Mode' on the confocal microscope was enabled to excite the two fluorophores separately in order to minimize crosstalk. We used the above method to label the nNOS/RyR pair and the eNOS/RyR pair which were then imaged using confocal microscopy and structured illumination microscopy. The pseudo-color coding of the molecules are the following: red for RyR, green for nNOS, and cyan for eNOS.

The quality of antibody labeling was evaluated by the maintenance of cell morphology (for example, rod-like, clear striations), brightness of labeling, and uniformity of labeling. For example, in well-preserved and well-labeled cells, the peripheral RyR labeling produced a clean and smooth outline and the intercalated RyR units are clearly visible; the labeling is bright and uniformly distributed throughout the entire cell [50]. Examples of the cell images are shown in Fig. S5.

**In vitro measurements of CaMKII activity with the Camui sensor**

Design and synthesis of the wild-type, phosphorylation-resistant, and oxidation-resistant Camui constructs have been previously described [37]. HEK293 cells were cultured in Eagle's

medium plus 5% fetal bovine serum and penicillin/streptomycin for 24 hours and then transfected with plasmids encoding Camui (or a mutant isoform) using a mammalian transfection kit (Stratagene). After an additional 24 hours, Camui expression was checked by fluorescence microscopy. HEK cells expressing Camui were lysed in $Ca^{2+}$-free buffer containing 50 mM Tris-HCl buffer (pH 7.5), 5 mM $MgCl_2$, and protease inhibitors. Fluorescence measurements were performed using a MS SpectraMax plate reading spectrophotometer (Molecular Devices) with excitation and emission slits set to 4 nm, excitation wavelength set to 440 nm, emission wavelengths set to 477 nm ($F_{CFP}$) and 527 nm ($F_{YFP}$), respectively. The cytosolic fraction of the transfected HEK cells was diluted in Camui fluorescence was measured in the presence of 10 µM CaM and 200 µM $Ca^{2+}$. EGTA 1 mM was used to chelate $Ca^{2+}$ and autonomous CaMKII activity was measured in the presence of 1 mM EGTA and either 50 µM or 500 µM SNAP.

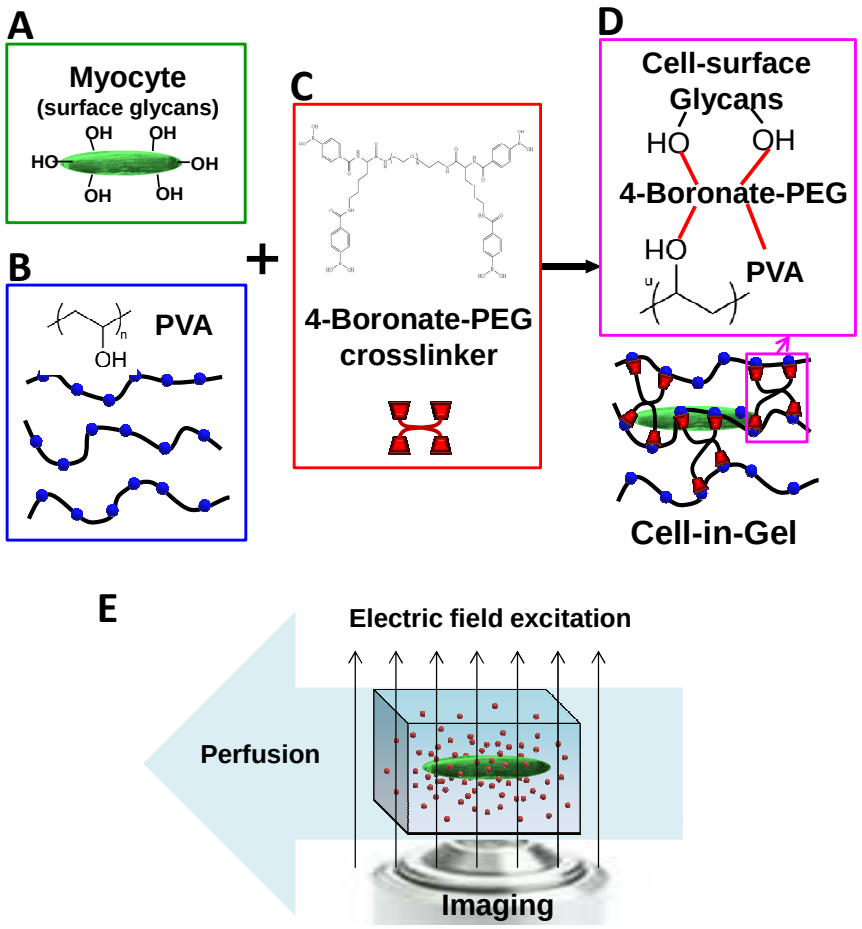


**Fig. S1. PVA–cross-linker system for embedding single cardiomyocytes in a 3D elastic matrix.** Schematic of a cardiomyocyte embedded in 3D PVA hydrogel matrix (Cell-in-Gel). First, the cell (***A***) was mixed with PVA solution (***B***); then 4-boronate-PEG cross-linker (***C***) was added. The boronate cross-links the cis-diols of the cell surface glycans to the PVA gel, thereby embedding the cell in the PVA gel with the cell surface tethered to the gel (***D***). ***E***) This Cell-in-Gel system allows solution exchange by perfusion to study drug effects, electric field stimulation to study excitation-contraction coupling in cardiomyocytes, and microscopic imaging to study the structure and function of embedded cardiomyocytes. Displacement in the gel can be tracked by embedded submicron fluorescent beads.

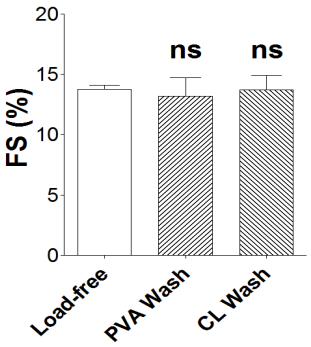


**Fig. S2. PVA or cross-linker alone did not affect contraction.** Fractional shortening (FS) of cardiomyocytes post-incubation in either PVA (n=27 cells) or cross-linker (CL, n=8 cells), in comparing to the load-free control in the normal Tyrode solution (n=6 cells). One-way ANOVA test show no significant difference (p=0.86).

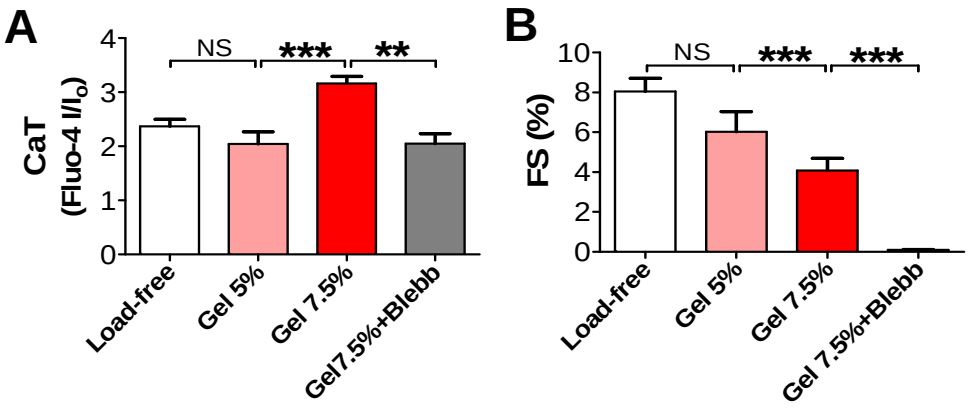


**Fig. S3. Mechanical stress effects on the systolic $Ca^{2+}$ transient and contraction.** Cardiomyocyte contraction and systolic $Ca^{2+}$ transient (CaT) were measured using Fluo-4 confocal imaging. Shown are **(A)** the peak CaT and **(B)** the fractional shortening (FS=% of sarcomere length change) in cardiomyocytes contracting load-free (n=18 cells), in softer gel made of 5% cross-linker (Gel5%, n=9), in harder gel with 7.5% cross-linker (Gel7.5%, n=18), and after blebbistatin treatment (n=5). One-way ANOVA with Bonferroni post-test is used for pair-wise comparison: P<0.05*, P<0.01** P<0.001*** deemed significant, and P>0.05 non-significant (NS).

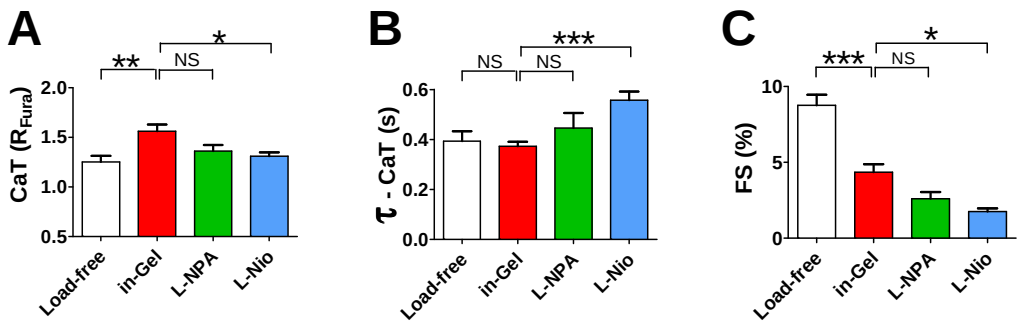


**Fig. S4. Effect of inhibiting nNOS or eNOS on cardiomyocytes.**
$Ca^{2+}$ transient and cardiomyocyte contraction were simultaneously measured using Fura-2 ratio ($R_{fura}$) and the sarcomere detection method. (A) The peak systolic $Ca^{2+}$ transient (CaT), (B) Tau of the $Ca^{2+}$ transient decline, and (C) fractional shortening contraction (FS=% of sarcomere shortening) in cardiomyocytes contracting load-free (n=22), in-Gel (n=18) and after treatment with L-NPA to inhibit nNOS (n=7) or treatment with L-Nio to inhibit eNOS (n=12). One-Way ANOVA test show significant difference in CaT ($p<0.05$), Tau ($p<0.01$), and FS ($p< 0.001$); Bonferroni post-test is used for pair-wise comparison between the in-Gel group and the others: $P<0.05$*, $P<0.01$**, $P<0.001$*** deemed significantly different with the confidence level of 95%.

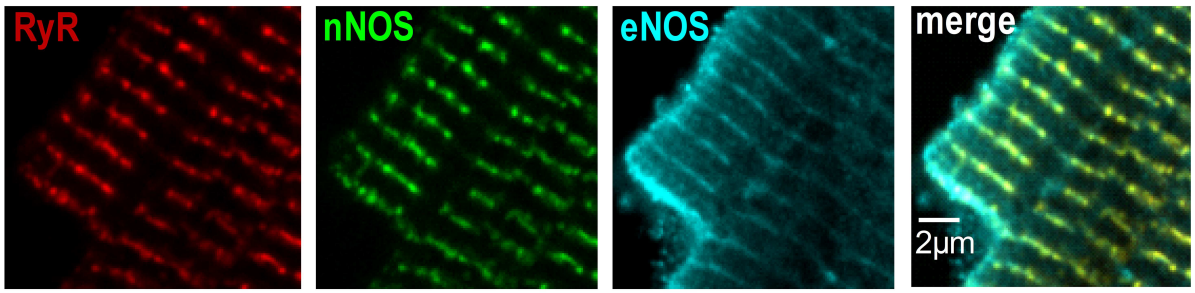


**Fig. S5. Distribution of RyR, nNOS, and eNOS in a wild-type cardiomyocyte.**
Sample confocal images acquired with a 60X water immersion objective, NA=1.2, Zoom=10 ( n=20 cardiomyocytes from 3 individual animals).

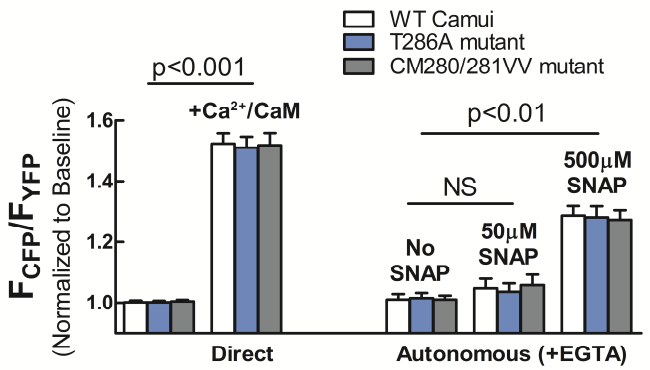


**Fig. S6. NO-dependent activation of CaMKII.**
FRET measurements using the Camui sensor show direct activation of wild-type, non-auto-phosphorylatable (T286A), and non-oxidizable (CM280/281/VV) mutant CaMKII by $Ca^{2+}$/CaM (two sets of bars at the left). When the intracellular concentration of $Ca^{2+}$ was dropped by treatment with EGTA, the activation of CaMKII was decreased (bars labeled No SNAP). Autonomous CaMKII activation occurred by with a SNAP concentration of 500μM but not 50 μM. Notably, the SNAP/NO-dependent autonomous activation is not secondary to either phosphorylation or oxidation, consistent with a direct effect of NO on CaMKII**.** n=6 samples in each bar. One-way ANOVA with Bonferroni post-test was used for pair-wise comparison; p value shows the significance of difference between each pair (same color) under different conditions.

**Movie S1. Cell-in-gel contraction.**

The movie was recorded using a high speed camera (1 KHz) attached to an IonOptix system mounted on an Olympus IX71 inverted microscope with water immersion objective 40X, NA=1.2, corrected for the thickness of No.1 glass coverslip.

**Movie S2. 3D rendition of nNOS-RyR colocalization.**

This movie shows a 3D rendition of the super-resolution fluorescence images of antibody-labeled nNOS (green) and RyR (red) in a mouse ventricular myocyte obtained using structured illumination microscopy (SIM). SIM was done using a DeltaVision OMX V3.0 Blaze system (Applied Precision Inc, a GE Healthcare Company, Issaquah, WA). 3D rendering of the SIM images was done using the Volocity plus Visualization package.

**Movie S3. 3D rendition of eNOS-RyR distribution.**

This movie shows a 3D rendition of the SIM super-resolution fluorescence images of antibody-labeled eNOS (cyan) and RyR (red) in a mouse ventricular myocyte.

Science Signaling
AAAS

# ` Mechano-Chemo Transduction Tunes the Heartstrings

Benjamin L. Prosser and Christopher W. Ward (18 March 2014)
*Science Signaling* **7** (317), pe7. [DOI: 10.1126/scisignal.2005214]

CELL BIOLOGY

# Mechano-Chemo Transduction Tunes the Heartstrings

**Benjamin L. Prosser[1]* and Christopher W. Ward[2,3]***

**In the beating heart, mechanical stretch triggers the production of reactive oxygen or nitrogen species that target $Ca^{2+}$-signaling proteins. Termed mechano-chemo transduction, this pathway "tunes" the calcium release machinery in the healthy heart; when dysregulated, it contributes to disease. In this issue of *Science Signaling*, Jian *et al.* used a "cell-in-gel" method to show that contractions in healthy heart cells elicit a steep, viscosity-dependent increase in mechano-chemo transduction in which nitric oxide synthase (NOS), NADPH oxidase 2 (Nox2), and $Ca^{2+}$/calmodulin-dependent kinase II (CaMKII) contribute. These authors provide evidence for a role of neuronal NOS (nNOS) over endothelial NOS; they supported their findings with super-resolution microscopy, which localized nNOS nearest to the $Ca^{2+}$ release sites. In a disease model, signaling through nNOS and CaMKII rather than through Nox2 was enhanced, supporting the independent mechano-activation of these enzymes. The coupling of these quantitative approaches will provide a new understanding of mechano-chemo transduction.**

More than 60 years ago, Sandow coined the term excitation-contraction (EC) coupling and proposed cytosolic calcium as the critical activator of muscle contraction (*1*); it has now become clear that contraction itself provides important feedback in shaping this calcium signal. In this issue of *Science Signaling*, Jian *et al*. extend the concept of mechano-chemo transduction, a term that encompasses how mechanical stress dynamically modulates calcium handling through chemical effectors (*2*). Jian *et al*. showed the utility of a tool in which they embedded cardiomyocytes in a variable-viscosity gel that interacts with the cell membrane. The "cell-in-gel" contracts under viscoelastic load with stress transmitted in three dimensions (*3*). Using this technique, they identified neuronal nitric oxide synthase (nNOS), NADPH oxidase 2 (Nox2), and $Ca^{2+}$/calmodulin-dependent kinase II (CaMKII) as key enzymes involved in the mechanical modulation of EC coupling and raise intriguing questions about the mechanism involved. Here, we offer a mechanistic discussion and testable hypotheses for future work aimed at defining the interplay of cell mechanics and calcium signaling in healthy and diseased myocardium.

Key players in cardiomyocyte mechano-chemo transduction are located in the dyad (Fig. 1), the intersection between a junctional sarcoplasmic reticulum (jSR) and transverse tubule. The type 2 ryanodine receptors (RyR2s) cluster in the jSR membrane, directly opposed to L-type calcium channels in the t-tubule, and are activated by calcium-induced calcium release. The importance of RyR2 regulation is underscored not simply by its role in releasing $Ca^{2+}$ stores to drive contraction, but also because abnormal RyR2 activity contributes to $Ca^{2+}$-dependent arrhythmias, hypertrophy, and heart failure. At the dyad, previously established regulators of RyR2 function include nNOS and endothelial NOS (eNOS), both of which produce NO; Nox2, which produces superoxide that is rapidly dismuted to hydrogen peroxide, resulting in ROS in the dyadic space; and CaMKII.

The principal finding of Jian *et al*. is that compared to myocytes contracting under little or no load, cell-in-gel contractions increased global calcium release and led to a high frequency of $Ca^{2+}$ sparks (*4*) without detectably changing SR calcium content. Although this finding is consistent with enhanced activation of RyR2, simple pump-leak balance (*5*) would suggest that SR $Ca^{2+}$ content should decrease, thereby implicating additional factors. The authors also propose that the enhanced RyR2 activation contributes to the Anrep effect, the slow augmentation of calcium release and contractility that occurs with an increase in cell stress (*6*).

Furthermore, the authors identified NOS as a key regulator of the augmented response. Although this result extends the work of the Solott group and others (*7*), the use of pharmacologic agents and genetic ablation revealed that nNOS rather than eNOS was the dominant chemoeffector, and super-resolution imaging showed colocalization of nNOS near the RyR2s. This combination of live-cell and super-resolution imaging sets a new standard for examining the microdomain signaling of these molecules.

Nox2 or CaMKII inhibition were equally effective to nNOS inhibition in blocking mechanically induced activation of RyR2 during cell-in-gel contractions. This confirms reports from our group and others showing that Nox2-generated ROS (X-ROS) is a potent mechano-chemoeffector of RyR2, but also raises the question of apparently redundant signaling.

One possibility is that Nox2 and NOS are triggered by separate mechanical stimuli that are each activated during cell-in-gel contractions. X-ROS signaling is activated by longitudinal and axial stresses through the microtubule cytoskeleton (*2*, *8*, *9*), whereas NOS is modulated by membrane shear stress through yet-unidentified elements. As modeled (*10*), a cell-in-gel contraction results in both longitudinal and axial stress as well as three-dimensional shear stress at the membrane. This provides a parsimonious explanation for dual activation of NOS and Nox2 in the cell-in-gel experiments, yet incompletely explains their redundant roles.

Another nuance of the cell-in-gel system that may contribute to augmented signaling is the steep, nonlinear dependence of RyR2 activation on gel density. In fact, healthy cells contracting in the denser gel exhibited very high $Ca^{2+}$ spark frequencies consistent with destabilized RyR2s more commonly seen in disease models. Although we speculate that the stiffer gel may more closely approximate supraphysiologic stress, the signaling generated in these experiments has resulted in important new findings. A critical next step is to define the viscoelastic environment of the healthy and diseased heart in situ; with these parameters, the gel can be adjusted to evaluate cardiomyocytes under pathophysiologic and physiologic stresses. An additional advancement would be the ability to apply diastolic stretch to the cell-in-gel system to separate the effects of preload and afterload stress, as each may have different effects on downstream signaling.

[1]Department of Physiology, Perelman School of Medicine, University of Pennsylvania, Philadelphia, PA 19104, USA. [2]Department of Organizational Systems and Adult Health, University of Maryland School of Nursing, Baltimore, MD 21201, USA. [3]Center for Biomedical Engineering and Technology (BioMET), University of Maryland School of Medicine, Baltimore, MD 21201, USA.

*Corresponding author. E-mail: ward@son.umaryland.edu (C.W.W.); bpros@mail.med.upenn.edu (B.L.P.)

Jian *et al*.'s investigation into an arrhythmia model arising from a troponin T (TnT) mutation reveals that similar stresses may elicit different signaling depending on the pathophysiological background. In contrast to healthy cells, the cell-in-gel enhancement of RyR2 activation in TnT mutant myocytes was dependent on NOS and CaMKII but independent of Nox2—a finding that supports independent activation pathways. However, in a dystrophin-deficient cardiomyopathy model, the microtubule cytoskeleton is stiffened and Nox2 abundance is increased; consistently, microtubule-dependent Nox2 hyperactivation underlies the $Ca^{2+}$ instability induced by preload stress (*2*). Results in disease states will undoubtedly correlate with the abundance and regulation of the key mechanosensitive enzymes and transducers; without this information, it is difficult to place the TnT mutant results in context.

Regardless of the activation stress, signaling interactions among nNOS, Nox2, and CaMKII likely contribute to their apparently equal enhancement of RyR2 activation (Fig. 1B). Nox2-generated superoxide, which becomes $H_2O_2$, can directly oxidize and activate RyR2, as can NO. However, superoxide can also interact with NO to form peroxynitrite, which also modifies target proteins such as RyR2. CaMKII is a likely player in this pathway because it can be activated by oxidation by Nox2-ROS (*11*) and NO (*12*). Synergism among Nox2, NOS, and CaMKII has become increasingly evident. We find that with frequent passive stretches, X-ROS production dominates RyR2 modulation initially (within seconds), but NOS and CaMKII signaling arise after a delay (tens of seconds) (*13*). Consistent with this finding, Dries *et al*. reported that Nox2-dependent activation of CaMKII likely underlies RyR2 modulation during high-frequency mechanical stress (*14*).

An additional target of this synergistic interplay not addressed by Jian *et al*. is the mechanosensitive channel (MSC) (Fig. 1). MSCs are modulated by both ROS and NO and are implicated in the Anrep effect. X-ROS activation of MSCs contributes to increased cytosolic calcium during mechanical stress (*9*) and may contribute to the RyR2 activation reported here. The role of NO is more complex: Kass and co-workers have demonstrated that activation of protein kinase G, which is driven by NO, suppresses MSC activity to blunt the Anrep effect (*15*). Initially, this appears in opposition to the results presented by Jian *et al*., which suggest that NO augments the Anrep effect through modulation of RyR2; how can these seemingly disparate results be reconciled?

First, bear in mind that mechano-chemo transduction depends on the nature of the mechanical stress and abundance of key players. Studies using various methods of stress in complex disease models require both independent and unified interpretation. Although mechanotransduction in the cell-in-gel system is currently uncalibrated and complex, it is a methodological approach that makes measuring mechanotransduction accessible to the scientific community. However, there are still two issues to reconcile: (i) the conflicting role of NO as a modulator of the Anrep effect, and

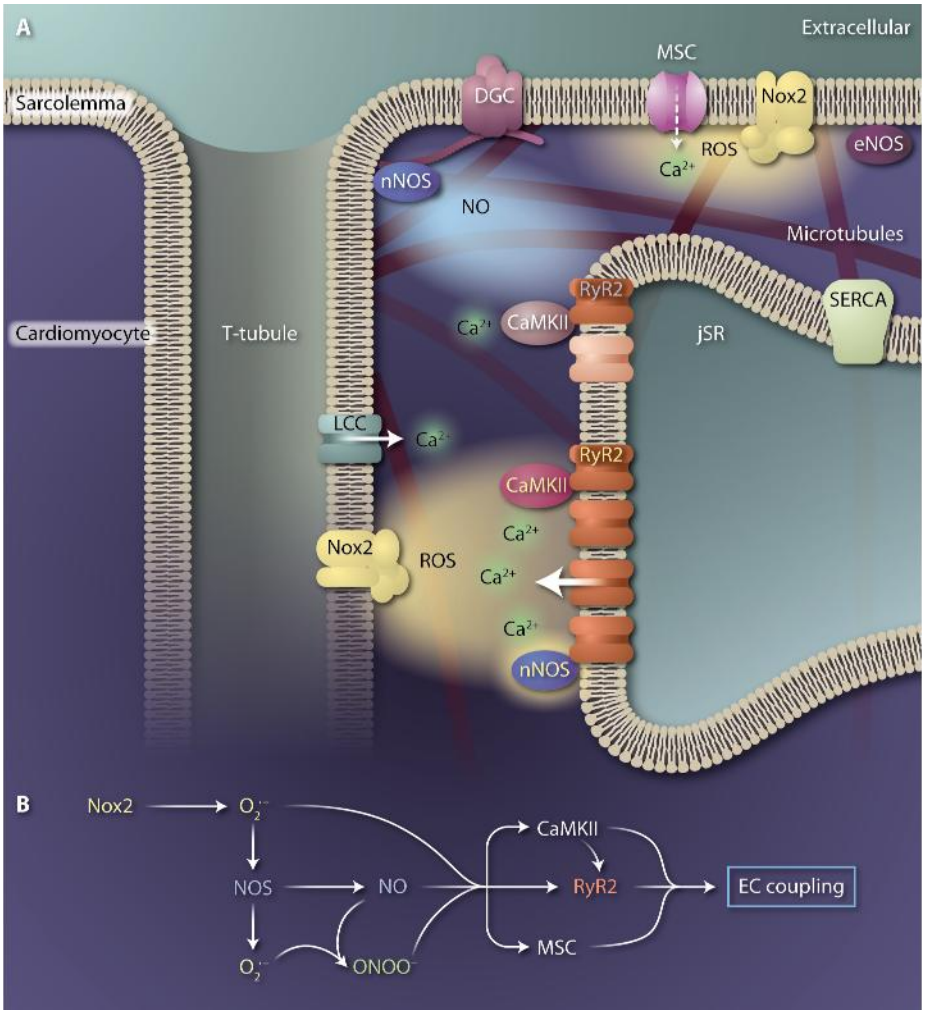


**Fig. 1. Mechano-chemo transduction in the heart.** (**A**) Simplified model of key players at the calcium release unit of a cardiomyocyte. Upon mechanical stress, mechanosensitive enzymes generate local signals that target calcium handling proteins. These include Nox2, which produces ROS in the sarcolemmal and T-tubule membrane, and NOS, which produces NO and is localized to the SR and sarcolemma membranes as part of the dystrophin-dystroglycan complex (DGC). ROS and NO can directly regulate RyR2 activity through oxidation and nitrosylation, respectively, or can activate CaMKII, which modulates RyR2 through phosphorylation. Superoxide in the subspace can uncouple nNOS, resulting in superoxide rather than NO production. Superoxide and NO can also interact to form peroxynitrite. Additional targets of ROS and NO include the mechanosensitive channel (MSC), the L-type $Ca^{2+}$ channel (LCC), and the sarcoplasmic/endoplasmic reticulum $Ca^{2+}$ ATPase (SERCA). ROS and NO preferentially modify target proteins in their immediate vicinity, as depicted by the sensitized RyR2 and CaMKII (in darker colors). Although mechano-chemo coupling tunes EC coupling in the healthy heart, altered localization or expression of key players underscores the destabilized calcium signaling seen with increased mechanical stress and in disease. (**B**) Potential linear reaction schemes involved in mechano-chemo transduction.

CREDIT: H. MCDONALD/*SCIENCE SIGNALING*

(ii) the seemingly redundant effects of Nox2, CaMKII, and nNOS on EC coupling. We thus propose a conceptual hypothesis to unify both unresolved issues (Fig. 1).

In the presence of superoxide, nNOS becomes "uncoupled" and switches from NO to superoxide production (*16*). We hypothesize that healthy cells contracting in a stiff viscous gel will generate substantially more Nox2-ROS, which can uncouple nearby nNOS, leading to an additional source of superoxide. Both superoxide sources may then directly modify RyR2 and synergistically effect EC coupling through CaMKII (Fig. 1). This would explain the redundant effects seen by Jian *et al*., while also separating the influence of NO from uncoupled nNOS (and thus ROS) on the Anrep effect. New work with the cell-in-gel and complementary approaches will enable direct testing of this and alternative hypotheses in healthy and diseased heart.

Regardless of the nature or magnitude of stress, the study of Jian *et al*. highlights the importance of conducting experiments under mechanical load. Mechanical stress clearly influences calcium signaling, and studies in unloaded myocytes present a valuable but incomplete story. The new tools and questions stemming from the work of Jian *et al*. show that exciting discoveries await those who study mechano-chemo transduction.

**References**


1. A. Sandow, Excitation-contraction coupling in muscular response. *Yale J. Biol. Med.* **25**, 176–201 (1952).
2. B. L. Prosser, C. W. Ward, W. J. Lederer, X-ROS signaling: Rapid mechano-chemo transduction in heart. *Science* **333**, 1440–1445 (2011).
3. Z. Jian, H. Han, T. Zhang, J. Puglisi, L. T. Izu, J. A. Shaw, E. Onofiok, J. R. Erickson, Y.-J. Chen, B. Horvath, R. Shimkunas, W. Xiao, Y. Li, T. Pan, J. Chan, T. Banyasz, J. C. Tardiff, N. Chiamvimonvat, D. M. Bers, K. S. Lam, Y. Chen-Izu, Mechanochemotransduction during cardiomyocyte contraction is mediated by localized nitric oxide signaling. *Sci. Signal.* **7**, ra27 (2014).
4. H. Cheng, W. J. Lederer, Calcium sparks. *Physiol. Rev.* **88**, 1491–1545 (2008).
5. A. W. Trafford, M. E. Díaz, G. C. Sibbring, D. A. Eisner, Modulation of CICR has no maintained effect on systolic $Ca^{2+}$: Simultaneous measurements of sarcoplasmic reticulum and sarcolemmal $Ca^{2+}$ fluxes in rat ventricular myocytes. *J. Physiol.* **522**, 259–270 (2000).
6. G. von Anrep, On the part played by the suprarenals in the normal vascular reactions of the body. *J. Physiol.* **45**, 307–317 (1912).
7. M. G. Petroff, S. H. Kim, S. Pepe, C. Dessy, E. Marbán, J. L. Balligand, S. J. Sollott, Endogenous nitric oxide mechanisms mediate the stretch dependence of $Ca^{2+}$ release in cardiomyocytes. *Nat. Cell Biol.* **3**, 867–873 (2001).
8. G. Iribe, C. W. Ward, P. Camelliti, C. Bollensdorff, F. Mason, R. A. B. Burton, A. Garny, M. K. Morphew, A. Hoenger, W. J. Lederer, P. Kohl, Axial stretch of rat single ventricular cardiomyocytes causes an acute and transient increase in $Ca^{2+}$ spark rate. *Circ. Res.* **104**, 787–795 (2009).
9. R. J. Khairallah, G. Shi, F. Sbrana, B. L. Prosser, C. Borroto, M. J. Mazaitis, E. P. Hoffman, A. Mahurkar, F. Sachs, Y. Sun, Y.-W. Chen, R. Raiteri, W. J. Lederer, S. G. Dorsey, C. W. Ward, Microtubules underlie dysfunction in duchenne muscular dystrophy. *Sci. Signal.* **5**, ra56 (2012).
10. J. Shaw, L. Izu, Y. Chen-Izu, Mechanical analysis of single myocyte contraction in a 3-D elastic matrix. *PLOS ONE* **8**, e75492 (2013).
11. J. R. Erickson, M.-L. A. Joiner, X. Guan, W. Kutschke, J. Yang, C. V. Oddis, R. K. Bartlett, J. S. Lowe, S. E. O'Donnell, N. Aykin-Burns, M. C. Zimmerman, K. Zimmerman, A.-J. L. Ham, R. M. Weiss, D. R. Spitz, M. A. Shea, R. J. Colbran, P. J. Mohler, M. E. Anderson, A dynamic pathway for calcium-independent activation of CaMKII by methionine oxidation. *Cell* **133**, 462–474 (2008).
12. D. A. Gutierrez, M. Fernandez-Tenorio, J. Ogrodnik, E. Niggli, NO-dependent CaMKII activation during β-adrenergic stimulation of cardiac muscle. *Cardiovasc. Res.* **100**, 392–401 (2013).
13. B. L. Prosser, C. W. Ward, J. P. Kerr, G. Shi, W. J. Lederer, Stretch-dependent regulation of calcium signaling in heart—Who are the key players? *Biophys. J.* **106**, 322a (2014).
14. E. Dries, V. Bito, I. Lenaerts, G. Antoons, K. R. Sipido, N. Macquaide, Selective modulation of coupled ryanodine receptors during microdomain activation of CaMKII in the dyadic cleft. *Circ. Res.* 10.1161/CIRCRESAHA.113.301896 (2013).
15. K. Seo, P. P. Rainer, D. I. Lee, S. Hao, D. Bedja, L. Birnbaumer, O. H. Cingolani, D. A. Kass, Hyperactive adverse mechanical-stress responses in dystrophic heart are coupled to TRPC6 and blocked by cGMP-PKG modulation. *Circ. Res.* 10.1161/CIRCRESAHA.114.302614 (2014).
16. J. Sun, L. J. Druhan, J. L. Zweier, Dose dependent effects of reactive oxygen and nitrogen species on the function of neuronal nitric oxide synthase. *Arch. Biochem. Biophys.* **471**, 126–133 (2008).


10.1126/scisignal.2005214

**Citation:** B. L. Prosser, C. W. Ward, Mechano-chemo transduction tunes the heartstrings. *Sci. Signal.* **7**, pe7 (2014).